GUSTAVO CARAVITA DE ANDRADE

ROTOR FOR A TRANSVENTRICULAR BLOOD PUMP

São Paulo

2019

GUSTAVO CARAVITA DE ANDRADE

ROTOR FOR A TRANSVENTRICULAR BLOOD PUMP

Dissertation presented to the Post Graduation Program in Mechanical Engineer, of The University of São Paulo as a requirement to obtain Master Degree in Science.

Field of Study: Control and Mechanical Automation Engineering

Supervised by Prof. Dr. Oswaldo Horikawa

São Paulo

2019

Este exemplar foi revisado e corrigido em relação à versão original, sob responsabilidade única do autor e com a anuência de seu orientador.

São Paulo, _____ de _____ de _____

Assinatura do autor: _____

Assinatura do orientador: _____

Catalogação-na-publicação

Andrade, Gustavo
Rotor for a Transventricular blood pump / G. Andrade -- versão corr. -- São Paulo, 2019.
69 p.

Dissertação (Mestrado) - Escola Politécnica da Universidade de São Paulo. Departamento de Engenharia Mecânica.

1.Dinamica dos Fluidos 2.Método dos elementos finitos 3.Dispositivos De Assistência Ventricular I.Universidade de São Paulo. Escola Politécnica. Departamento de Engenharia Mecânica II.t.

Nome: Andrade, Gustavo Caravita

Título: Rotor for a Transventricular blood Pump

Aprovado em:

Banca Examinadora

Prof. Dr. _____

Instituição: _____

Julgamento: _____

Prof. Dr. _____

Instituição: _____

Julgamento: _____

Prof. Dr. _____

Instituição: _____

Julgamento: _____

ACKNOWLEDGEMENTS

I dedicate this work firstly to God, because he is essential in my life, to my father Aron, my mother Silvia for the ability to believe in me and support me.

I thank my colleagues, for the encouragement and for the constant support and all those who have been in some way close to me, making this life worth more and more.

Thank my girlfriend Jackeline who never denied support, care and encouragement. Thank you for putting up with so many stress and anxiety crises. Without you by my side this work would not be possible.

I am grateful to all the teachers who contributed to my academic trajectory, especially to Prof. Dr. Oswaldo Horikawa, responsible for guiding my project and for guiding me throughout the master's program, for the valuable advices, suggestions and criticisms, for sharing their experiences and for all the trust deposited. Thank you for clarifying so many questions and being so attentive and patient.

I thank Dr. Evandro Drigo for his friendship and knowledge.

I thank the friends of the Center of Engineering in Circulatory Assistance of the Dante Pazzanese Institute of Cardiology: Bruno Utiyama, Jeison Fonseca, Pérsio Aníbal, Rafael Nunes and Edir Leal

I thank the institutions that collaborated to carry out this work: CNPq, FAPESP, Nucleus of Fluid Dynamics of the Polytechnic School of USP, Dante Pazzanese Institute of Cardiology and Adib Jatene Foundation.

RESUMO

Segundo a Organização Mundial de Saúde, as doenças cardiovasculares(DCVs) são a causa número um de mortes em todo o mundo, exceto na África, onde a Síndrome da Imunodeficiência Adquirida é a principal causa de morte. Nesse cenário, o dispositivo de assistência ventricular (DAV) permanece como a única alternativa para prolongar a vida do paciente até o transplante cardíaco. No Instituto Dante Pazzanese de Cardiologia (IDPC), iniciou-se uma pesquisa e desenvolvimento de um DAV de Fluxo axial para ser totalmente implantável dentro do coração. Esta bomba, denominada Dispositivo de Assistência Transventricular (DATV), poderá ser implantada cirurgicamente através de uma pequena incisão intercostal esquerda de maneira minimamente invasiva. O objetivo desta pesquisa é desenvolver e analisar o fuso do DATV visando as melhores condições para auxiliar o funcionamento do sistema circulatório e evitar ao máximo as áreas de Fluxo recirculante, estagnação de Fluxo e elevadas tensões de cisalhamento no fluido por meio de técnicas de Dinâmica dos Fluidos Computacional (CFD) e testes *In Vitro*. São comparados rotores com diferentes tipos de aletas, eles se diferenciam pela curvatura e quantidade das aletas, baseando-se na literatura. São realizados estudos para determinar a importância de aletas na carcaça do DATV, concluindo que a carcaça com aletas é melhor, proporcionando Pressão e Fluxo maiores em menores rotações. São também realizados estudos sobre a influência da redução do *gap* entre o topo da aleta e a carcaça, esta redução aumentou a Pressão manométrica, porém houve um aumento significativo na tensão de cisalhamento. Os estudos mostram que o rotor com o melhor desempenho foi o rotor com 2 aletas dispostas a 180º, contínuo (apenas uma coluna de aletas) e com o passo da aleta sendo constante, o rotor 1Rev. Isto sugere que, para este dispositivo: (I) quanto maior o passo da pá, maior a carga de pressão, menor a vazão e aumenta a tensão de cisalhamento; (II) um passo variável diminui a eficiência da bomba e (III) uma lâmina não contínua diminui significativamente o desempenho hidrodinâmico da bomba e diminui a tensão de cisalhamento. Este rotor permitiu ainda atingir, a 12.500 rpm, uma altura manométrica máxima de 126 mmHg e uma vazão máxima de 4,5 L/min. Espera-se um baixo índice normalizado de hemólise (INH).

Palavras-chave: bomba de Fluxo axial, dispositivo de assistência ventricular, simulação computacional, estudo fluidodinâmico.

ABSTRACT

According to the World Health Organization, cardiovascular diseases (CVDs) are the number one cause of death worldwide, except in Africa, where Acquired Immunodeficiency Syndrome is the leading cause of death. In this context, the continued development of new devices to assist blood pumping until the transplant, has great value. The Dante Pazzanese Institute of Cardiology (IDPC, São Paulo, Brazil) has recently started a research and development project aiming an axial flow blood pump to be fully implanted within the heart. This pump, called Transventricular Assist Device (TVAD), can be implanted surgically through a small left intercostal incision in a minimally invasive manner. The objective of this research is to develop and analyze the rotor of the TVAD, aiming at the best conditions to support the circulatory system and to achieve: minimum areas of recirculating/stagnating flow and minimum shear stresses. The study is conducted through Computational Fluid Dynamics (CFD) and *In Vitro* tests. Based on literature, a sort of rotors featuring different geometries and number of blades are defined and tested. The hydrodynamic characteristics of the rotors are compared each other so as to determine the best one. Besides, studies are performed to determine the importance of volute vanes in the TVAD pumping characteristics. Finally, studies are carried out to verify the influence of the gap reduction between the periphery of the blade and the volute on the pumping characteristics as well on the hemolysis. The study showed that the rotor that presented the best performance were the rotor with two blades of constant pitch arranged each other at 180º. Suggesting that, for this device: (I) the higher the blade pitch, the higher the pressure load, the lower flow rate, and increases shear stress; (II) a variable pitch decrease the pump efficiency and (III) a non-continuous blade decreases significantly the pump's hydrodynamic performance and decreases the shear stress. At this speed, the maximum manometric head was of 126 mmHg and a maximum flow rate of 4.5 L/min. It is expected to have a low normalized index of hemolysis (NIH).

Keywords: ventricular assist device, transventricular, axial flow pump, impeller, Computational Fluid Dynamics.

LIST OF FIGURES

Figure 1 - Schematic drawing of TVAD placement in the left ventricle. 16
Figure 2 - Exposure time vs Shear curve..... 24
Figure 3 - 3D models of the rotors 1Rev, 2Rev, Gold and Debakey..... 29
Figure 4 - 3D models of the rotors 4_2, Em2 and Em3. 29
Figure 5 - 3D model of the TVAD. 30
Figure 6 - Formation of unified domains. 31
Figure 7 - Fluid Domain. 31
Figure 8 - Auxiliary Domain. 31
Figure 9 - Stationary and Rotational Fluid Domain. 32
Figure 10 - Mesh generated by the software 33
Figure 11 - Detail of the boundary layer..... 34
Figure 12 - Velocity profile around a point in the boundary layer. 34
Figure 13 - Pressure distribution over the volute 38
Figure 14 - 3D axial pump model (a) without volute vanes and (b) with volute vanes. 39
Figure 15 - Flow visualization inside the volute with vanes at 12500 rpm and 3 L/min. 39
Figure 16 - Flow visualization in the volute without vanes in the same conditions, 12500 rpm and 3 L/min. 40
Figure 17 - Pressure - Flowrate characteristic curves for volute with and without vanes obtained by simulation. 41
Figure 18 - Pressure Vs. Flow Curve to Rotor 1Rev. 43
Figure 19 - Pressure Vs. Flow Curve to Rotor 2Rev. 43
Figure 20 - Pressure Vs. Flow Curve to Rotor 4_2. 44
Figure 21 - Pressure Vs. Flow Curve to Rotor Golden Ratio. 44
Figure 22 - Pressure Vs. Flow Curve to Rotor Debakey. 45
Figure 23 - Pressure Vs. Flow Curve to Rotor Em2. 45
Figure 24 - Pressure Vs. Flow Curve to Rotor Em3. 46
Figure 25 - Plotted values 47
Figure 26 - Recirculation profile at 5500rpm for (A) 1Rev, (B) 2Rev, (C) Debakey, (D) Em3. 49
Figure 27 - Recirculation profile at 12500rpm for (A) 1Rev, (B) 2Rev, (C) Debakey, (D) Em3. 49
Figure 28 - Pressure Distribution on the volute (A) 1Rev, (B) Em3. 50
Figure 29 - Flow analysis for the rotor with gap of (A) 0.46 mm and (B) 0.30 mm. 51
Figure 30 - Comparative gap influence curve. 51
Figure 31 - (a) Volute without vanes and (b) Volute with vanes. 53
Figure 32 - Different geometries of rotors to be tested. 53
Figure 33 – Valves..... 54
Figure 34 - Motor cover, axle and rotor mounted near the motor. 54
Figure 35 - Assembled Prototype..... 55
Figure 36 - Evaluation Unit combined with the HCSS 56
Figure 37 - Exploded view of the EU. 56
Figure 38 - Performing the test 58
Figure 39 - Polygraph 58
Figure 40 - Digital tachometer 59
Figure 41 - Use of digital tachometer for speed measurement. 59

Figure 42 - Pressure Vs. Flow Curve to Rotor 1Rev - In Vitro 61
Figure 43 - Pressure Vs. Flow Curve to Rotor 2rev - In Vitro..... 61
Figure 44 - Pressure Vs. Flow Curve to Rotor Debakey- In Vitro 62
Figure 45 - Pressure Vs. Flow Curve to Rotor Em3 - In Vitro 62
Figure 46 - Comparative chart of the blood analogous fluid..... 64

LIST OF TABLES

Table 1 - Models of axial pumps and summary of some parameters. 19
Table 2 - Values of NIH and its clinical results. 23
Table 3 - Shear stress and exposure time for rupture of the red cell. 23
Table 4 - Velocity components. 25
Table 5 - Table with number of nodes used in the simulation. 35
Table 6 - Performed simulations. 37
Table 7 - Simulation data. 42
Table 8 - Shear stress and exposure time for each rotor. 47
Table 9 - In Vitro tests data. 60

NOMENCLATURES

Superscripts

®/™	Trademark

****

Abbreviations

CFD	Computational Fluid Dynamics
CVFEM	Control-Volume Finite Element Method
VAD	Ventricular Assist Device
TVAD	Transventricular Assist Device
CVD	Cardiovascular Diseases
EbFVM	Element-based Finite Volume Method
HF	Heart Failure
NIH	Normalized Index of Hemolysis
P1	Inlet Pressure
P2	Outlet Pressure
PFH	Plasma Free Hemoglobin
HCSS	Hybrid Cardiovascular System Simulator

****

Acronyms

CEAC	Center of Engineering in Circulatory Assistance
USA	United States of America
EPUSP	Polytechnic School of University de São Paulo
FAJ	Adib Jatene Fundation
IDPC	Dante Pazzanese Institute of Cardiology
Inc.	Incorporation
ISO	International Organization for Standardization
Ltda.	Limited
WHO	World Health Organization

****

Latin Words

In Vitro	Laboratory tests with appropriate equipment simulating real conditions
et. al	Among others

****

Symbols

ΔP	Difference between inlet and outlet pressure

****

Unit of Measurement

mmHg	Millimeters of mercury
L/min	Liters per minute
rpm	Rotation per minute
%	Percentage
min	Minute
s	Second
g/100L	Grams per 100 Liters
Pa	Pascal
g/mL	grams per milliliter
kg/s	kilogram per second
atm	atmosphere

SUMARY

Sumary ***13***

1. INTRODUCTION ***14***

1.1. Objectives **16**

1.1.2. Justification **17**

1.2. Methods **17**

2. LITERATURE REVIEW ***19***

2.1. Ventricular Assist Device (VAD) **19**

2.2. Rotor Geometry **20**

2.3. Hemolysis and Thrombosis **22**

2.4. Computational Fluid Dynamics (CFD) **24**

3. THREE-DIMENSIONAL MODELING AND ROTOR DESIGN ***28***

4. CFD ANALYSIS ***30***

4.1. Influence of Volute Vanes **38**

4.2. Fluidodynamic Analysis **41**

4.3. Shear Stress **46**

4.4. Flow Analyses **48**

4.5. Gap Influence **50**

5. IN VITRO TESTS ***52***

5.1. Construction of Prototypes of the TVAD **52**

5.2. Development of an Evaluation Unit **55**

5.3. Conducting the Tests **56**

5.4. Blood Analogous Fluid Testing **63**

6. CONCLUSION ***65***

7. REFERENCES ***66***

1. INTRODUCTION

Cardiovascular diseases (CVDs) are the leading causes of death in most countries in the world, with the exception of Africa, where AIDS (Acquired Immune Deficiency Syndrome) is the leading cause of death (Avezum *et al*, 2012). According to the World Health Organization - WHO, cardiovascular diseases are the number one cause of death worldwide. More people die annually from cardiovascular disease than from any other cause. It is estimated that 17.5 million people died of cardiovascular disease in 2012, accounting for 31% of all global deaths (WHO, 2017).

Among CVDs, heart failure (HF) is characterized by a syndrome in which the cardiovascular system has difficulties in maintaining the necessary perfusion to the tissues and organs, reducing patient's quality of life and considerably increasing mortality (Souza, 2012). Despite the pharmacological advances available to HF patients, many will need additional treatments, such as cardiac transplantation (Dinkhuysen *et al*, 2012).

However, ventricular assist devices or temporary mechanical circulatory supports remain as the only alternative to increase patient survival until the heart transplantation and is a viable treatment for end-stage HF (ISO 14708-5, 2010). In this context, the continued development of new devices, helping the heart to pump blood until the transplant, becomes of great value.

The development of blood pumps goes through design steps, prototype construction, *In Vitro* evaluation, *In Vivo* evaluation, clinical evaluation and release for use. These items are included in the international standard ISO 14708 - Implants for Surgery - Active implantable medical devices - Part 5: Circulatory support devices, 2010 (ISO 14708-5, 2010). This standard deals with a regulatory item of definitions, specifications, tests and documentation for the development of all procedure, this standard is already applied in Brazil as ABNT NBR ISO 14708-5: 2017.

Artificial Ventricle or Ventricular Assist Device (VAD) is a univentricular blood pump used to support the diseased ventricle. It can be pulsatile or continuous in terms of flow condition, as well, centrifugal or axial flow in terms of pumping principle. VAD is most often used for the left ventricle, but two devices can be used simultaneously in the case of biventricular assistance. For this last type of application, independent set of pump and controller is used for each ventricle. The VADs are medium to long-term devices to support

the patient's life, assisting the natural heart in pumping the blood throughout the care period (Bock *et al*, 2008).

In pulsatile VADs, the blood flow occurs due to the movement of a diaphragm associated with the use of artificial (mechanical or biological) valves, allowing the unidirectional passage of blood (Nosé *et al*, 2003). On the other hand, in non-pulsatile, or continuous flow VADs, the momentum is transferred from the rotor to the fluid directly (axial VAD) or through centrifugal force (radial VAD). Radial VADs promote a flow perpendicular to the rotational axis of the rotor, while Axial VADs, parallel to the rotational axis of the rotor (Leme, 2015).

Compared to radial pumps, axial pumps require higher rotor speed to achieve same amount of pressure and flow rate. However, the axial pump is much more compact. Because of their smaller size and tubular configuration, axial pumps require less time to implant, thereby reducing the invasiveness of the surgical procedure. Radial pumps usually weigh more than axial pumps. Therefore, such VADs may cause patient discomfort after the implant, in addition to normal complications during patient recovery. Furthermore, axial flow pumps generally consume less electrical power, which allows for more compact and lightweight power supply components and, eventually, implantable batteries (Song *et al*, 2003).

The applications of new technologies in the development of pumps aim to decrease the hemolysis (damage to the red blood cells) rate and the risk of thrombosis (formation of blood clot), with the improvement of the hydrodynamic performance and biocompatibility of their materials (Shankarraman *et al*, 2014).

In September 2016, the Dante Pazzanese Institute of Cardiology (IDPC) started a research and development project aiming an axial blood pump to be fully implanted within the heart. This pump, defined as Transventricular Assist Device (TVAD), will cross the left ventricle and aortic valve, pumping blood from the ventricle directly into the aorta artery. This concept, which is called also transvalvular, can be implanted surgically by a small left intercostal incision to give access to the apex of the left ventricle in a minimally invasive manner, reducing postoperative complications and facilitating the patient recovery, Figure 1.

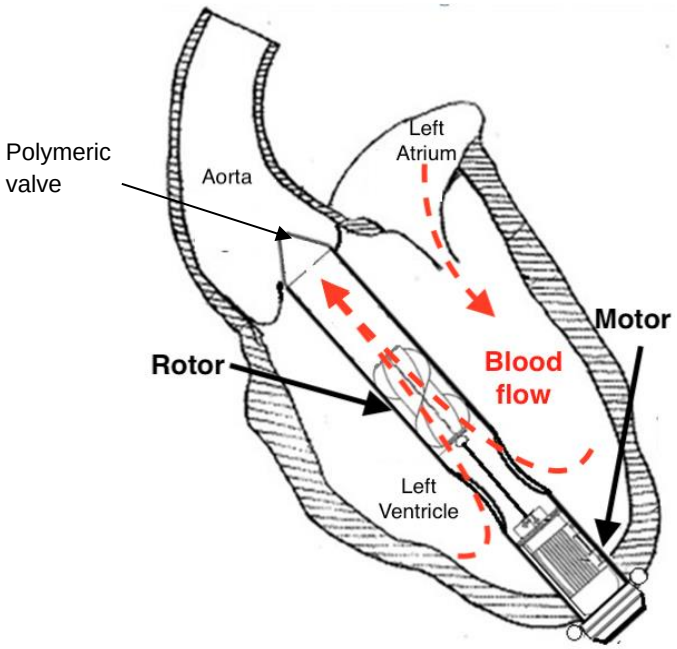

Figure 1 - Schematic drawing of TVAD placement in the left ventricle.

1.1. Objectives

The objective of this research is to develop and analyze the rotor of an axial blood pump aiming best conditions to assist the heart in pumping blood to circulatory system, minimizing areas of recirculating flow or flow stagnation and high shear stresses in the fluid. The study is developed using Computational Fluid Dynamics (CFD) numerical approach and *In Vitro* tests.

1.1.1. Specific objectives

- Proposal of different configurations of rotor for the implantable axial blood pump, through a three-dimensional modeling software;
- For each rotor, conduct the flow analysis, survey of the characteristic curves and shear stress analysis, using the Finite Volume Method, through a CFD software (ANSYS CFX);
- Construction of prototypes of the implantable axial blood pump using 3D printing technology;
- *In Vitro* tests with the prototypes to obtain Pressure versus Flow curves for different rotor speeds.

- Analysis of collected data, comparing the obtained results, to indicate the best model for the TVAD rotor.

1.1.2. Justification

Brazil is considered a country that has always followed the technological advances of cardiac surgery and has mortality rates compatible with those of the first world in this area. However, even with advances in cardiology and the development of new drugs, heart transplantation is the most appropriate treatment and, in some cases, the only treatment for patients with severe heart diseases (Silva, 2012). However, there are several difficulties in obtaining the organs to perform heart transplants and, given the large demand of patients, the most important cardiology research centers around the world are developing and using ventricular assist devices as a form of treatment for cardiovascular diseases, which has managed to minimize mortality related to these diseases (Nosé, 2003).

1.2. Methods

Three-dimensional models of the TVAD with different rotor geometries are elaborated through a 3D modeling software, so that the fluidodynamic analysis of the TVAD can be made using the Finite Volume Method, with the CFD software ANSYS CFX, aiming the best conditions to support the circulatory system, i.e., the highest physiological pressure and flow. When testing rotors with different geometries it might be concluded that rotors with higher pitch have higher flow when there is no restriction at the pump outlet and rotors with lower pitch have higher pressure gain at the pump outlet with the flow totally restricted;

Through the characteristic curves generated by the CFD, 4 rotors with the best conditions to support the circulatory system were chosen to be used in the following tests.

Prototypes of the implantable axial blood pump are built using 3D printing technology with the 4 chosen rotors, so that *In Vitro* tests can be performed to obtain pressure versus flow curves for different rotations (hydrodynamic performance curves) and consequently validation of the data obtained by CFD analyses.

Then, flow visualizations inside the pump are done, by CFD, to observe areas of recirculating flow and stagnant flow. When performing the visualization, the velocity and direction of the fluid is observed and, where the velocity is very low, there is the possibility of thrombus formation.

Lastly, flow analyses are performed, by CFD, and minimized high shear stresses in the fluid. A high shear stress with a high exposure time to this stress will cause a high Normalized Index of Hemolysis (NIH).

Hemolysis testing will not be performed as it involves handling fresh blood and this work will comprise only *In Vitro* evaluation and simulation of the TVAD performance.

2. LITERATURE REVIEW

In this chapter, it will be presented the theoretical framework that consists of the review of texts, articles, books and all relevant material for better understanding this study.

2.1. Ventricular Assist Device (VAD)

VADs can be pulsatile or non-pulsatile, and the second one can be radial or axial. The axial VAD can also be classified according to implantation surgical procedure: transcatheter (TC), open heart surgery (OHS) and minimally invasive surgery (MIS). In TC, the axial flow pump is inserted through the femoral artery and positioned, for example, inside aorta in order to increase arterial blood flow. In OHS, the surgeon makes a large incision at sternum bone, pulls the ribs apart and implants the VAD. The VAD can be either directly implanted to the ventricle or connected to the ventricle by cannula. MIS is an alternative to OHS, where surgeons can perform the procedure using laparoscopy or through very small incisions.

Table 1 shows some well-known models of axial VADs currently in use or under development, along with some parameters.

Table 1 - Models of axial pumps and summary of some parameters.

Model	Company	Pressure (mmHg)	Flow (L/min)	Rotation (rpm)	Types	Diameter (mm)
Valvo Pump	--	100	5	7,000	OHS	38
Streamliner	UPMC	100	6	7,000	OHS	--
INCOR I®	Berlin Heart	100	5	8,000	OHS	30
HeartMate II™	Thoratec Corporation	100	4	9,000	OHS	40
Jarvik 2000®	JarvikHeart Inc.	100	7	12,000	OHS	25
DeBakey VAD®	Micromed	100	6	12,500	OHS	25
IVAP	SUN Med. Tec. Corp.	--	8	13,000	OHS	13.5
LongHorn	HeartWare Inc.	60	6	21,000	MIS	20
Hemopump	Medtronic Inc.	--	5	26,000	TC	8.1
Impella®	Abiomed	100	7	30,000	TC	6.4

Source: adapted from Song *et al*, 2003 and Connellan *et al*, 2013.

The company HeartWare (Massachusetts, USA) is developing the "Longhorn" pump, a new VAD that is in the pre-clinical testing stage. The device requires minimal surgical access for transmiocardial implantation. It does not have a valve at the outlet, but it is operated at high speeds so as to inhibit the return of flow during diastole. The Longhorn is capable of supplying up to 6 L/min of flow to support the ventricle. According to Connellan *et al*, 2013, a surgery was performed using a pig model in cardiopulmonary bypass. Longhorn was implanted in the right ventricle through its diaphragmatic surface. The outflow cannula was directed to the main pulmonary artery and a severe biventricular dysfunction was induced by the connection of the right and left main coronary arteries. The device allowed the successful disuse of cardiopulmonary bypass. Flows of 3.4 L/min were generated with the rotor at 18,000 rpm, resulting in a mean arterial pressure of 60 mmHg. Longhorn can fully support the right ventricle (Connellan *et al*, 2013).

Like Longhorn, the TVAD will be implanted by MIS. Different of Longhorn, TVAD will use a valve at its outlet. Thus, it will not need to generate a large pressure load during the diastolic phase to avoid reverse flow through the pump (Andrade *et al*, 2017). Consequently, it can operate at a relatively low speed. It is expected that the TVAD will reach flow up to 3 L/min under a load up to 80 mmHg, with the rotor at speeds below 13,000 rpm, sufficient values for a VAD to work properly.

2.2. Rotor Geometry

The optimization of flow machines ranges from the selection of materials to the definition of the best shapes for the blades and their positioning on the rotor. Many papers in the literature evaluate the optimization of these machines from different points of view, obtaining results that show significant efficiency gains. For example, in Wen-Guang, 2011, an inverse problem-based methodology is used to design pump rotor blades, performing simulations in CFD to measure hydrodynamic performance and obtaining results that demonstrate efficiency improvements of around 5%.

There is a large amount of data in the literature demonstrating the efficiency of the CFD study in minimizing hemolysis and thrombosis. The ABNT NBR ISO 14708-5: 2010 standard proposes computer simulation as a tool for validation of circulatory support

devices. It determines test guidelines seeking results in hydrodynamic performance, hemolysis or thrombus formation.

Regarding the rotor design, the first relevant aspect is related to the pitch, i.e., the distance between two consecutive blades. A low blade pitch results in high pumping pressure and low flow (Sudhamshu *et al*, 2016).

According to Mizuguchi *et al*, 2008, rotors with continuous blades, that is without any division in the blade, result in the elimination of zones of high negative pressure, reducing hemolysis in the pump. However, according to Wampler, 1987, the best combination of blades consists of a non-continuous rotor with three blades spaced 120 degrees apart and divided into two columns. The three-bladed arrangement provides the best compromise between flow orientation and drag loss. To confirm which model is the best, tests were performed on both, continuous and a column-divided rotor.

The number of blades in the rotor appears to be a relevant factor in the study of the efficiency of flow machines, as the intuition leads to the belief that a larger number of propellers allows a higher interaction between rotor and fluid and thus allows a better transfer of energy. However, experiments presented in Gölcü, 2005, show that efficiency tends to decrease as the numbers of blades is increased, since there is a bottleneck in the flow between the blades and an increase in friction between the fluid and the structure in the paths between the blades, with the highest losses occurring due to the congestion generated at the rotor inlet. The usual number of blades is between 2 and 8 (Kanpur, 2018).

In terms of gap between the rotor and the pump housing, in an axial turbine, such gap is generally around 1% to 2% of the blade height. An increase in the gap implies in an increase in fluid leakage and consequent degradation of the pump performance (Schabowski et al, 2007 apud Oliveira, 2014). However, a change in the gap will promote important changes in the shear stress in the fluid, so it is necessary to find the best combination between performance and shear stress.

2.3. Hemolysis and Thrombosis

Artificial pumping of blood requires certain precautions due to the problems generated by this type of procedure. Inconveniences related to blood pumping concern the formation of clots or thrombosis, trauma to the blood cells and the formation of bubbles inside the devices are reported by Nosé et al, 1971. Those problems must be minimized and conducted to physiologically acceptable levels (Nosé, 1971).

Blood clotting has long been known to involve three factors, the Virchow triad: the nature of the surface, the condition of the blood, and local flow conditions. Slow, stagnant or recirculating flow and low shear stress promote thrombosis (Hochareon *et al*, 2004).

A problem commonly associated with blood pumping is the occurrence of hemolysis, i.e., a rupture of the red blood cell membrane, releasing hemoglobin into the plasma, constituting plasma free hemoglobin (PFH). Hemoglobinuria is the phenomenon generated by the increase of PFH, as a consequence of hemolysis (Silva et al, 2013). A high concentration of PFH can cause kidney dysfunction (Olsen, 2000).

The hemolysis rates depend on the levels of stress to which the cells are submitted and the time of exposure of these cells to the agents that cause trauma (Legendre *et al*, 2003).

Hemolysis occurs when the product of shear stress acting on the cell and the exposure time to this shear stress exceeds a critical threshold (Leverett *et al*, 1972).

When developing a blood pump, it is desirable to maintain the NIH (Normalized Index of Hemolysis) at values that do not cause clinical problems for the patient. It is important to evaluate these values during the blood pump development process, so that design changes can be made if necessary (Chan *et al* 2014). The NIH values and their corresponding clinical results are shown in Table 2 (Nosé, 1998 and Chan *et al*, 2014).

Table 2 - Values of NIH and its clinical results.

NIH (g/100L)	Clinical Results
>0,06	Increased level of PFH
>0,04	No increase in PFH, but requires blood transfusion
<0,04	Physiologically satisfactory
<0,02	Clinically satisfactory
<0,01	Ideal level for extended mechanical assistance

Fonte: Nosé, 1998 and Chan *et al*, 2014

Some parameters raised in Morales, 2017, considering the time of exposure of red blood cells to shear stresses. For that, the trajectories of the particles where the shear stress occurs were considered. Table 3 presents reference values of shear stress and exposure time that cause red blood cells rupture, according to the type of flow.

Table 3 - Shear stress and exposure time for rupture of the red cell.

Flow type	Exposure time (s)	Shear (Pa)
Laminar	$>10^{2}$	150
Turbulent	10^{2}	150
Laminar	10^{-1}	150-400
Turbulent	10^{2}	150-250
Laminar	10^{0}	400
Turbulent	$\leq 10^{-2}$	400
Turbulent	10^{-3}	450
Capillary	10^{-2}	500

Flow type	Exposure time (s)	Shear (Pa)
Capillary	10^{-2}	450~700
Turbulent	$\leq 10^{-2}$	≥600
Laminar	10^{-1}~10^{0}	600
Turbulent	10^{-3}	800
Turbulent	10^{-6}	1000
Turbulent	10^{-4}	1000
Turbulent	10^{-5}	4000
Turbulent	10^{-5}	4000

An Exposure time vs Shear curve was generated with these values, Figure 2, the area in blue represents the values where there is no mechanical induced hemolysis.

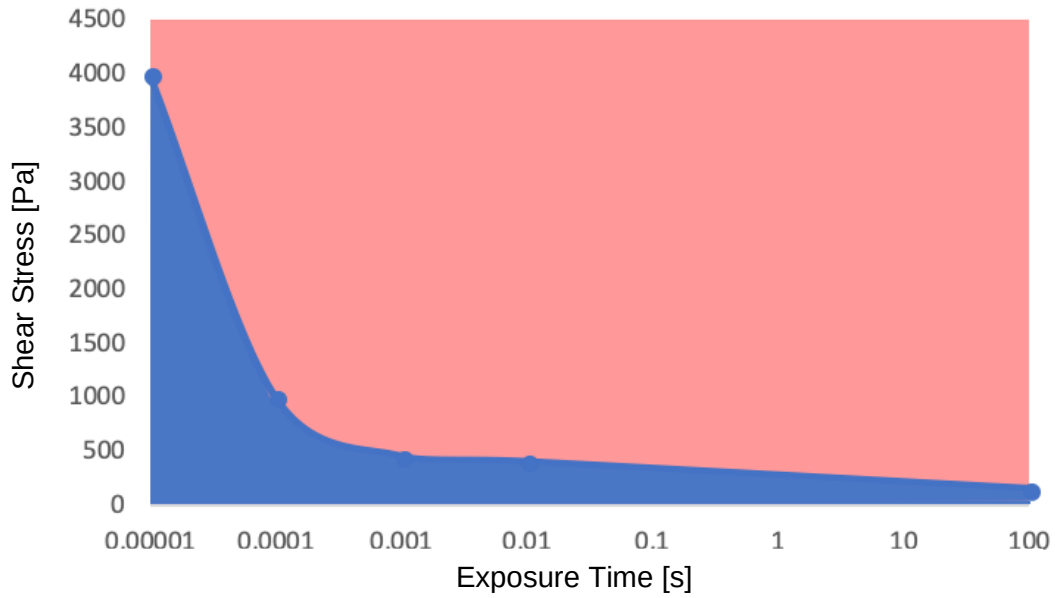

Figure 2 - Exposure time vs Shear curve.

2.4. Computational Fluid Dynamics (CFD)

Computational simulation for fluid flow problems is commonly referred as CFD (Computational Fluid Dynamics). The simulation of a diversity of types of flow pumps is made from CFD tools to assist in their projects, promoting an increase in their performance (Gulich, 1999, Burgreen *et al*, 2001, Voorde *et al*, 2004).

The element based finite volume method was originally developed to solve flows described by the Navier-Stokes equations. The methods general idea was initially proposed in Baliga *et al*, 1980, in the early eighties, for the solution of advection-diffusion equations. Later, the methodology was extended by these same authors to solve more general problems of fluid mechanics and heat transfer (Baliga *et al*, 1983). In these works, unstructured meshes of triangular elements were considered as a geometric base to build control volumes by joining the centroids of each triangle with the midpoints of its sides. The differential conservation equations were integrated into each of these control volumes to obtain approximate equations that respected the conservation of physical quantities at the discrete level. These authors also proposed the name Control-Volume Finite Element

Method (CVFEM) for this method. However, as argued in Maliska, 2004, this denomination is imprecise, since it suggests that it is a method that follows the philosophy of the finite element method and that also employs control volumes. However, as mentioned above, the reality is that it is a method built on the conceptual basis of the finite volume method and that only uses the element concept for the geometric representation of the solution domain. For this reason, the name Element-based Finite Volume Method (EbFVM) is more appropriate, which is used in this paper.

The software used in fluid flow simulations is ANSYS CFX, which uses the EbFVM. The equation that rules this simulation system is equation I, this is the integral form of the transport equation, it involves continuity, the amount of movement and the energy:

$$\underbrace{\frac{\partial}{\partial t}\int_{V}\rho\emptyset\, dV}_{\text{Transient}} + \underbrace{\oint_{A}\rho\emptyset\, V.dA}_{\text{Convective}} = \underbrace{\oint_{A}\Gamma_{\emptyset}\nabla\emptyset\,.dA}_{\text{Diffusive}} + \underbrace{\int_{V}S_{\emptyset}dV}_{\text{Root}} \qquad (I)$$

Where ∅ is the variable (described below as speed) transported through a site of density ρ and constant of diffusion Γ that moves in a volume V with a root term $S_{\emptyset}$.

The equation is the same as Navier Stokes, but applied to the amount of motion, values of the speed components (in each 3 dimensions) are then placed in the variable '∅'.

Table 4 - Velocity components.

Equation	∅
Continuity	1
X momentum	*u*
Y momentum	*v*
Z momentum	*w*
Energy	*i*

This formula is deduced by obtaining a control volume and for this volume a balance was made of continuity, amount of movement and energy.

This equation has a Transient term (which varies with time), Convective term, Diffusive term and a Root term (involves everything that does not adapt well to this common structure, to generalize these equations, is placed inside the root term).

In the equations below, it can be seen that there were divergents and gradients in the equation. It is the same equation, but in a discrete or not continuous way, not working with integral, because the computer does not solve them, so the equation is simplified from divergents and gradients (Maliska, 2004).

Continuity $$\frac{\partial \rho}{\partial t} + div(\rho u) = 0 \quad \text{(II)}$$

X momentum $$\frac{\partial (\rho u)}{\partial t} + div(\rho \mu u) = -\frac{\partial p}{\partial x} + div(\mu\ grad\ u) + S_{Mx} \quad \text{(III)}$$

Y momentum $$\frac{\partial (\rho v)}{\partial t} + div(\rho v u) = -\frac{\partial p}{\partial y} + div(\mu\ grad\ v) + S_{My} \quad \text{(IV)}$$

Z momentum $$\frac{\partial (\rho w)}{\partial t} + div(\rho w u) = -\frac{\partial p}{\partial z} + div(\mu\ grad\ w) + S_{Mz} \quad \text{(V)}$$

Energy $$\frac{\partial (\rho i)}{\partial t} + div(\rho i u) = -p\ div\ u + div(k\ grad\ T) + \Phi + S_i \quad \text{(VI)}$$

Where t is time, ρ is density and viscosity μ, which is constant for a Newtonian fluid and for a non-Newtonian fluid varies according to Carreau's law:

$$\mu = \mu_\infty + (\mu_0 - \mu_\infty)[1 + (\lambda\gamma)^2]^{\frac{n-1}{2}} \quad \text{(VII)}$$

The viscosity at high shear rate (μ_∞) is equal to the value for the Newtonian model (i.e., 0.0035 Pa.s) while the initial shear value (μ_0) is 0.25 Pa.s, the shear rate (γ) varies over time. And the relaxation time (λ) is 25s and the power index (n) is 0.25 according to Vosse, 1987. This equation will be used to calculate the effective shear stress for each rotor as proposed in Hernandes, 2017.

The ANSYS CFX software uses the EbFVM to convert the equations that rules the phenomena into expressions that can be numerically solved. The method consists of discretizing the spatial domain into finite control volumes using a mesh. The equations are integrated over each control volume, generating discrete equations that ensure the conservation of mass, amount of motion and energy for each control volume (ANSYS, 2007).

3. THREE-DIMENSIONAL MODELING AND ROTOR DESIGN

In this chapter, the three-dimensional models of the components of the TVAD and the rotors will be presented with descriptions of the differences in their geometries.

Three-dimensional models of an object can be obtained by different means and different softwares, where each one has its own way of representing surfaces and volumes. At the Circulatory Assistance Engineering Center (CEAC) of IDPC, an Axial Pump is being studied and developed to be used as a TVAD. Based on the requirements found in the literature already presented in this work, three-dimensional models of the pump were created to determine its external and internal geometries using a 3D modeling software, models that were used in computer simulation and prototype construction.

Simultaneously to the computational simulation, the three-dimensional models have been changed to obtain a better hydrodynamic performance.

As previously stated, the first relevant aspect is related to the pitch value, i.e., the distance between two consecutive blades. Low values of pitch result in high pumping pressure and low flow rate. To verify this aspect, two rotors are proposed: the 1Rev and the 2Rev (Figure 3 (a) and (b)). 1Rev and 2 Rev consider constant pitch, however a variable pitch should also be considered. Recently, researchers have begun to study the influence of golden ratio in cardiology, seeing that the rhythmic heartbeat follows a harmonic pattern (Sharif, 2014). Inspired in this study, here, a rotor in which the pitch varies accordingly to the golden ratio is proposed (Figure 3(c)). Also, the Debakey rotor, with a progressively varying pitch is also reproduced here (Figure 3(d)).

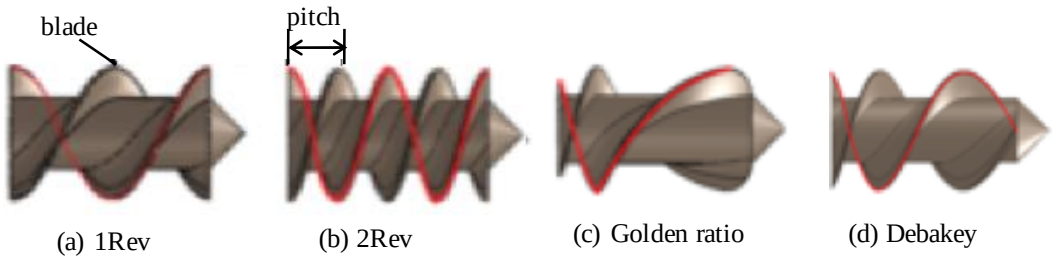

Figure 3 - 3D models of the rotors 1Rev, 2Rev, Gold and Debakey.

Above presented rotors contain a single continuous pitch rotor, without any division in the blade. Such rotors, according to some studies already presented, result in the elimination of zones of high negative pressure, reducing the hemolysis rate in the pump. However, according to Wampler, 1987, the best combination of blades consists of a non-continuous rotor with three blades spaced of 120 degrees divided in two columns. The three-blade arrangement provides the best compromise between flow orientation and drag loss. Therefore, in this study, tests were done also using a non-continuous rotor. Figure 4 shows the 3 non-continuous rotors created: the 4_2 (Figure 4(a)) with two segments, one with four blades of small pitch and 2 blades of large pitch; the Em2 (Figure 4(b)) with two segments, each containing 3 blades of large pitch and; the Em3(Figure 4(c)) with three segments, each containing 3 blades of low pitch.

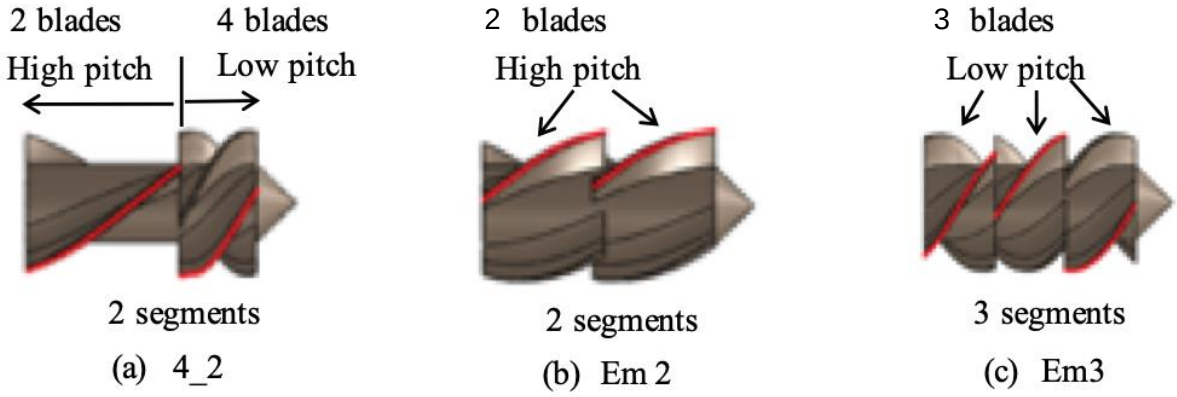

Figure 4 - 3D models of the rotors 4_2, Em2 and Em3.

The archives containing different rotor geometries were properly converted (.STL extension) to be sent to the 3D printer.

Besides rotor models, also models for the volute, polymeric valve, motor, shaft and motor cover were created. The TVAD geometries were based on the motor diameter and some heart dimensions. Here, a brushless and sensorless DC brushless motor (Maxon 404080) is considered. It presents: a nominal torque of 8.09 mNm, current at maximum torque of 1.68 A, nominal voltage of 24 V and nominal speed of 38,100 rpm. The three-dimensional models were prepared to be used in CFD analysis. After some tests, changes were made in the dimensions of the volute, such as the increase in the outlet diameter of the volute and the creation of fins at the inlet of the flow, as shown in Figure 5.

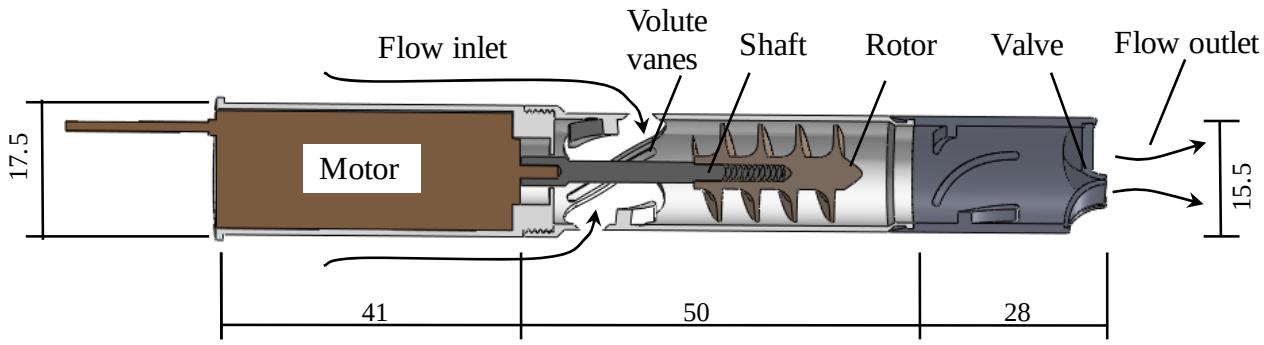

Figure 5 - 3D model of the TVAD.

4. CFD ANALYSIS

In this chapter, the steps for performing the fluid dynamics analysis will be presented, including the geometry simplification, generation and refinement of the mesh, the adopted boundary conditions, an analysis of the influence of the vanes in the volute, the pressure vs. flow curves for each rotor, an analysis of the shear stress in the fluid, an analysis of the flow inside the pump and the study of the influence of the gap.

To simplify the simulation, several changes were made to the geometries of the axial pump. In a first moment, two domains were formed, one between the shaft and rotor and another between the volute and the engine cover, according to Figure 6.

.

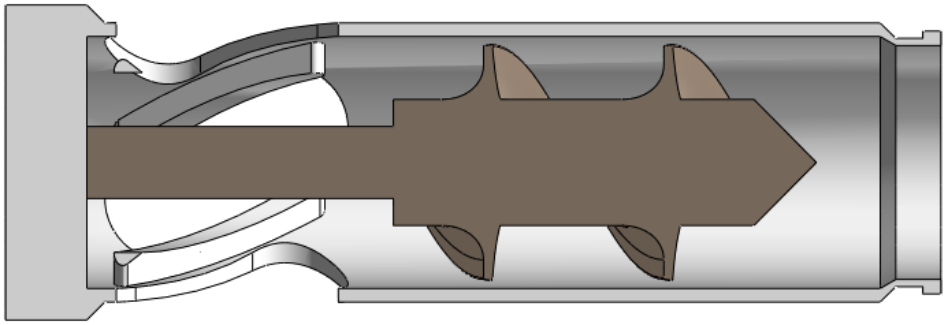

Figure 6 - Formation of unified domains.

From the creation of both domains, it was possible to extract the fluid domain, an element that represents the volume that will be occupied by blood inside the axial pump, according to Figure 7.

Figure 7 - Fluid Domain.

After the creation of the fluid domain, an intermediate domain was created, called auxiliary domain, to delimit what will be considered in rotational motion and what will be considered stationary, as shown in the Figure 8.

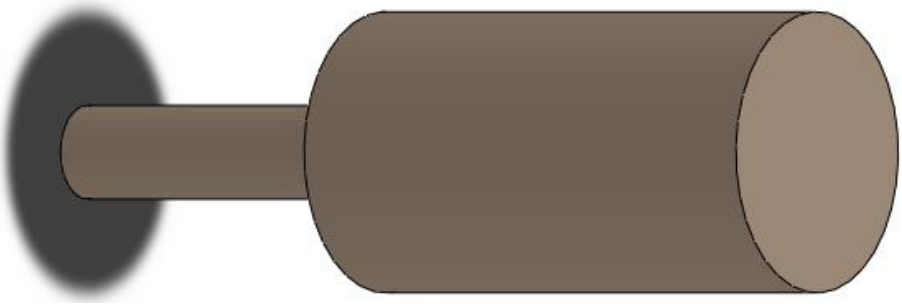

Figure 8 - Auxiliary Domain.

Then, a Boolean operation of subtraction of two bodies was performed between the auxiliary domain and the fluid domain, segregating the fluid domain into two bodies,

namely them: Stationary Fluid Domain and Rotational Fluid Domain, according to Figure 9.

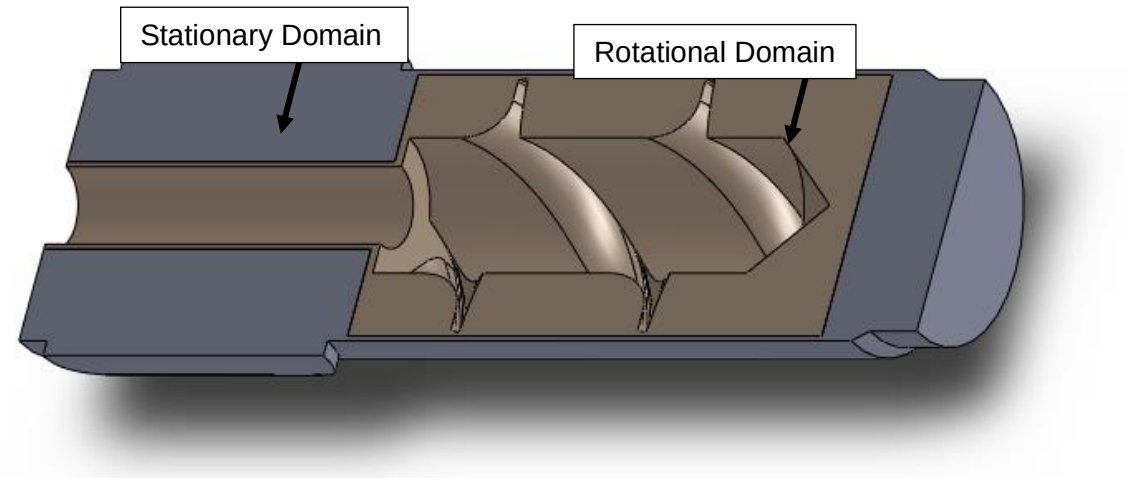

Figure 9 - Stationary and Rotational Fluid Domain.

The objective of segregation into two domains is to ensure that it is possible to assign velocity in all the fluid that is inside the stationary fluid domain, because it is not assigned velocity in the walls.

After the creation of the domains, the geometry was transferred to the mesh generator of the ANSYS software, as follows Figure 10.

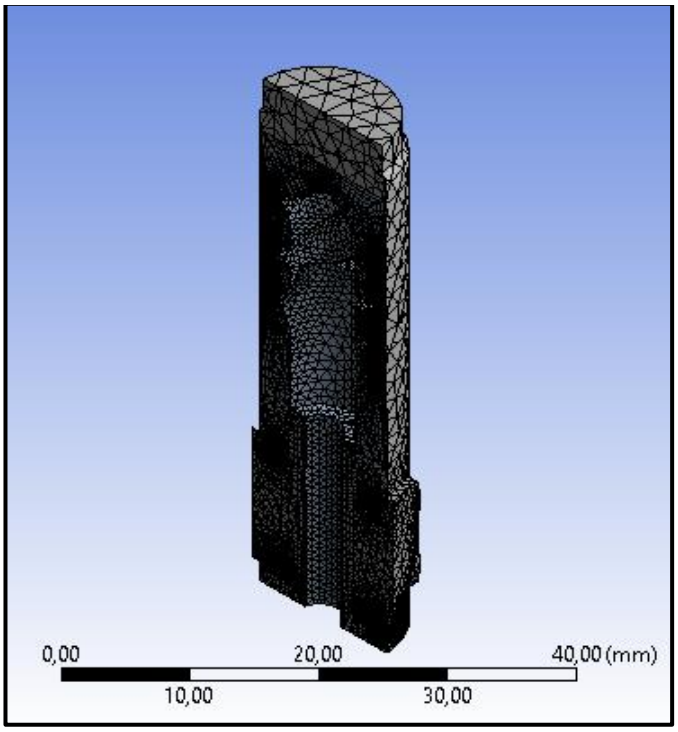

Figure 10 - Mesh generated by the software

Subsequently, the mesh in the walls was refined, Figure 11, according to the fluid mechanics theory, if observed a referenced point on the stationary surface, its velocity is equal to zero. With the increase of the distance (*y*) between the point and the wall, in a boundary layer analysis, the velocity (u) increases with a progressive variation until a certain moment, the velocity variation is no longer significant. Thus, the flow presents the nominal velocity of the center of the pipe. In this condition, there is a very high velocity gradient near the walls and, to capture this phenomenon, it is necessary to have a more refined mesh, according to Figure 12. The number of nodes and elements used in the simulation are described below, according to Table 5. Although some comparative tests have been made with more than one million nodes previously, this number of nodes proves efficient, and consuming little computational time, as the results converged with the in vitro tests.

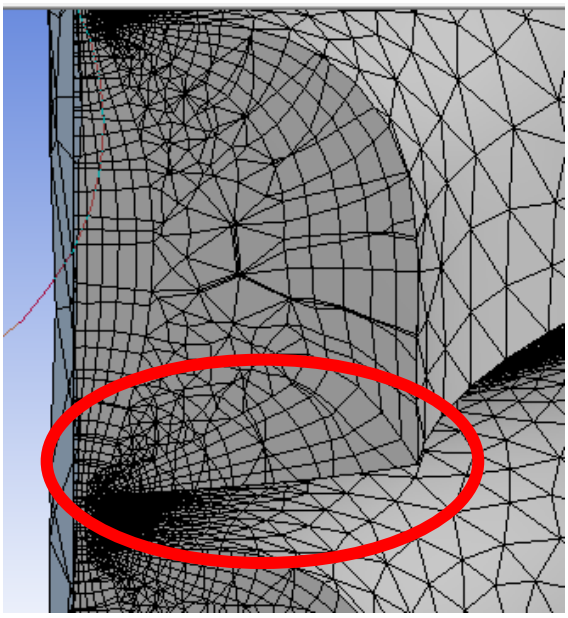

Figure 11 - Detail of the boundary layer.

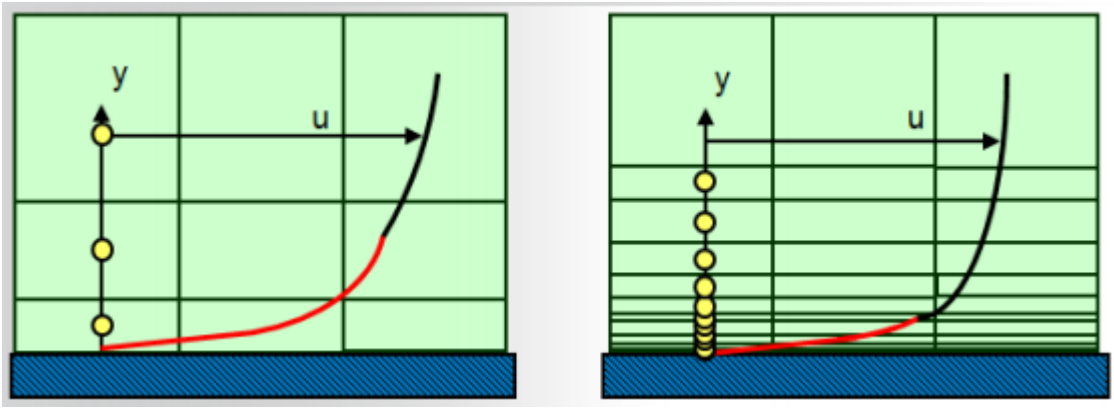

Figure 12 - Velocity profile around a point in the boundary layer.

Some parameter adjustments were made to the mesh configurations in order to avoid a very large number of nodes, increasing the computational cost and the time required to perform iterations. A maximum of 4 layers of the mesh were defined in the walls where there is contact with a solid (i.e., they will have 4 layers where there is contact with solids), the growth rate of these layers was defined as 1.2 (i.e., the next layer is 20% higher than the previous one), with smooth transition at a transition ratio of 0.77, the preference of the solution used for CFX and the size of the elements varies according to the curvature of the solid.

Table 5 - Table with number of nodes used in the simulation.

Rotor model	Number of nodes
1 Rev	591.534
2 Rev	650.916
4_2	706.265
Golden Ratio	553.283
Debakey	696.282
Em2	625.532
Em3	727.216

After all adjustments in the pump mesh, the parameterization of the boundary conditions to be considered in the fluid dynamics simulation was started.

The following parameters were considered to perform the simulation:

- The fluid to be used is water with a reference pressure of 1 atm;

- Stationary domain defined as stationary, without movement;

- Movement of the rotating domain defined as rotating and with angular velocity of 5500, 9000, 10300 and 12500 rpm.

- Axis of rotation defined as the geometrical axis of the rotor itself (Following the right-hand rule, the pump rotation is given by this axis);

- A fluid-fluid interface was created (because both sides of the interface are fluids), on the contact surfaces of the stationary fluid domain with the rotating fluid domain;

- The mixing model has been defined as Frozen Rotor as it is an optional configuration for rotary analysis that reduces simulation time and produces an approximate solution. The Frozen Rotor model treats the flow from one component to the next by changing the frame of reference while maintaining the relative position of the components and is useful for quickly simulating rotating devices without the complexity of numerically rotating the physical rotor. Frozen Rotor model analyses are generally faster

because the software does not update the position of the rotating mesh and the rotor-stator slider interface at each time step. As the rotor is stationary, larger time steps can be used, which lead to a stable state solution in less time (Autodesk, 2018).

- The flow inlet was defined in the stationary domain, according to the specification of the axial pump and perpendicular to the surface;

- Mass flow rate of 0.00832; 0.01664; 0.02496; 0.03328; 0.0416 and 0.04992 kg/s (Water mass conversion equivalent to 0.5; 1.0; 1.5; 2.0; 2.5 and 3 L/min, considering the water density of 0.998 g/mL).

- Inlet turbulence was determined as a 5% intensity average.

- The turbulence model was determined as K-epsilon and K-omega. There are different kinds of turbulence models: (i) the Spalart–Allmaras model was designed specifically for aerospace applications involving wall-bounded flows; (ii) the K-epsilon model is a two-equation model which gives a general description of turbulence by means of two transport equations, although doesn't perform well in cases of large adverse pressure gradients; (iii) the K-omega model attempts to predict turbulence by two partial differential equations for two variables, the turbulence kinetic energy (k) and (ω) is the specific rate of dissipation (Wilcox, 1998); (iv) the SST model combines the K-omega turbulence model and K-epsilon turbulence model such that the k-omega is used in the inner region of the boundary layer and switches to the k-epsilon in the free shear flow; (v) Reynolds stress equation model are the most complete classical turbulence model, the eddy-viscosity hypothesis is avoided and the individual components of the Reynolds stress tensor are directly computed, it uses the exact Reynolds stress transport equation for their formulation.

- It was defined in the stationary domain the flow output according to the specification of the axial pump, with a relative static pressure of 0Pa;

After the parameterization of all domains, the solution control was edited in two parameters for better simulation performance: (i) increase of the maximum number of

iterations to 1000 (so that it was not limited to the number of iterations) (ii) the residue in RMS generated by iterations to 0.0001

After the parameterization of the boundary conditions, the simulation process was started. For each rotor geometry, 19 simulations were performed, according to Table 6, related to the flow obtained by the *In Vitro* test. A total of 152 different simulations were executed in approximately 912 hours (~ 6 hours per simulation).

Table 6 - Performed simulations.

Rotations (rpm)	Flow (L/min)
5500	0.5
	1.0
	1.5
9000	0.5
	1.0
	1.5
	2.0
10300	0.5
	1.0
	1.5
	2.0
	2.5
	3.0
12500	0.5
	1.0
	1.5
	2.0
	2.5
	3.0

Following the simulation process, post processing was started for analyzing the results. Initially, the difference of the average pressure at the inlet and outlet in mmHg was calculated, according to Figure 13.

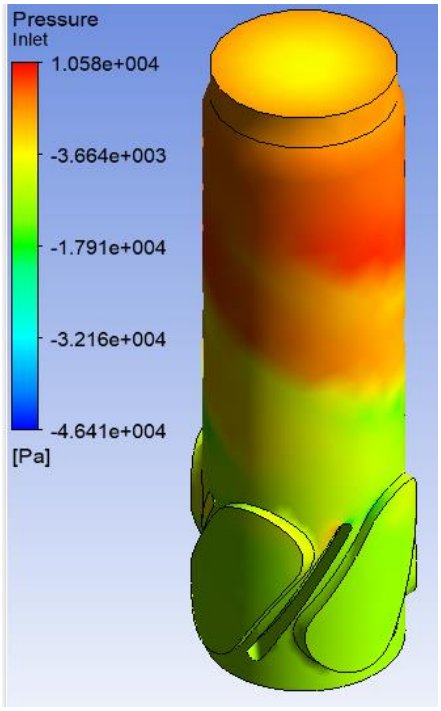

Figure 13 - Pressure distribution over the volute

The objective is to generate a Pressure (mmHg) x Flow (L/min) curve to make a comparison with the results obtained in the *In Vitro* test. Then, streamlines were created to visualize the flow in the inner part of the pump. Also, a plane with velocity vectors was created to analyze the direction and direction of the flow.

4.1. Influence of Volute Vanes

Based on the requirements found in the literature, two three-dimensional models of pumps were created, one with and the other without volute vanes, Figure 14. Using these models, a fluid dynamics analysis was performed.

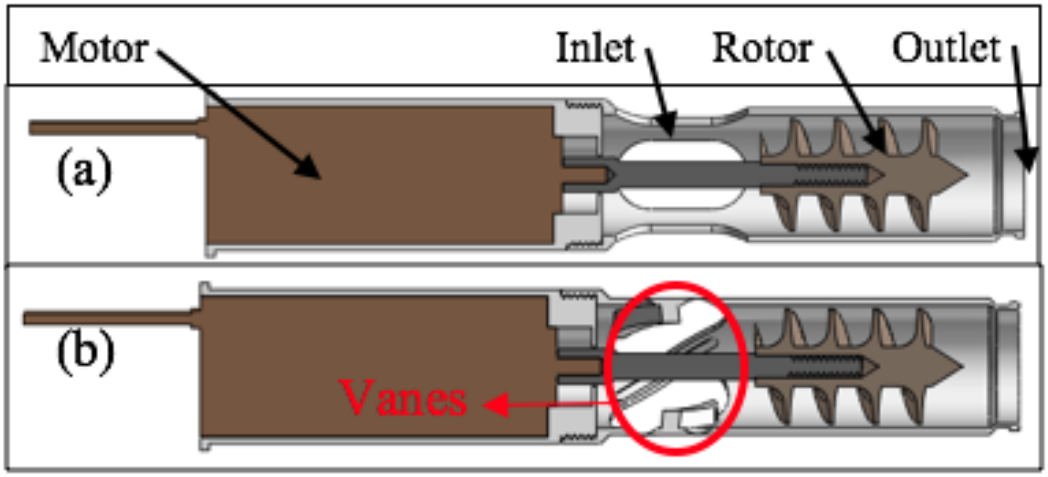

Figure 14 - 3D axial pump model (a) without volute vanes and (b) with volute vanes.

CFD Analysis shows that the presence of vanes in the volute ensures that most of the flow is directed to the rotor, while in the case of a volute without vanes, a large amount of liquid is recirculated within the pump volume. These two situations are illustrated respectively by the Figure 15 and Figure 16.

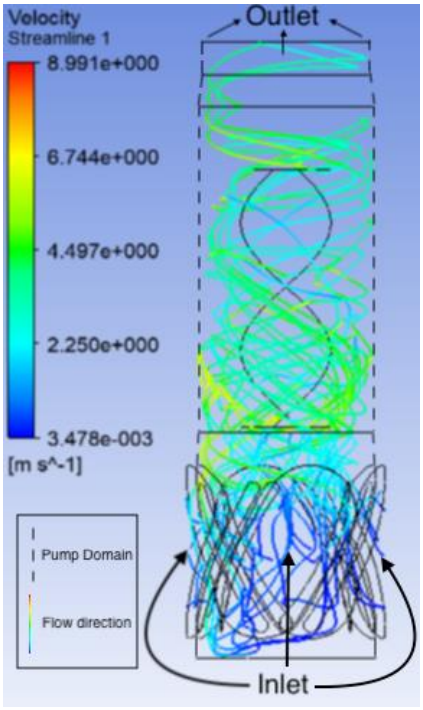

Figure 15 - Flow visualization inside the volute with vanes at 12500 rpm and 3 L/min.

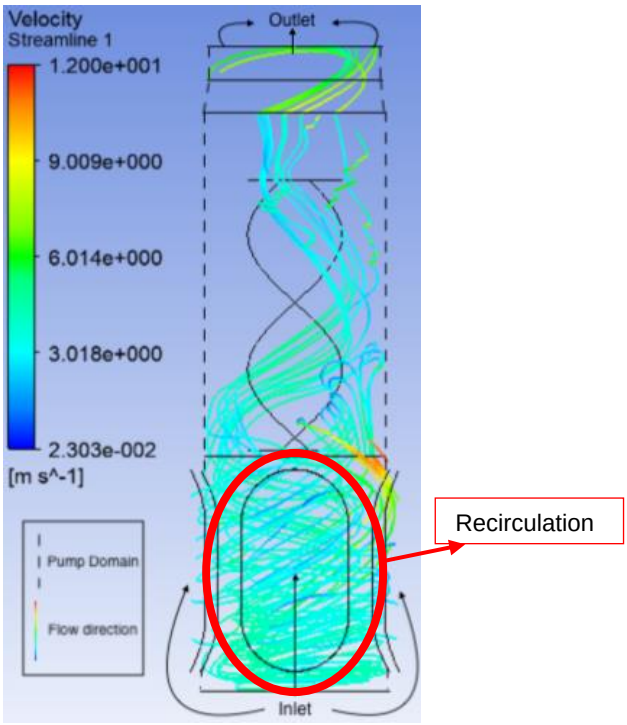

Figure 16 - Flow visualization in the volute without vanes in the same conditions, 12500 rpm and 3 L/min.

The analysis also shows that, as a consequence, the volute with vanes provides higher pressure and flow for the TVAD compared to the vaneless volute. This is observed with low or high flow values, and also with low or high speeds, but becomes more significant at high speeds. This comparison can be seen in the Pressure-Flow characteristic curves shown in Figure 17.

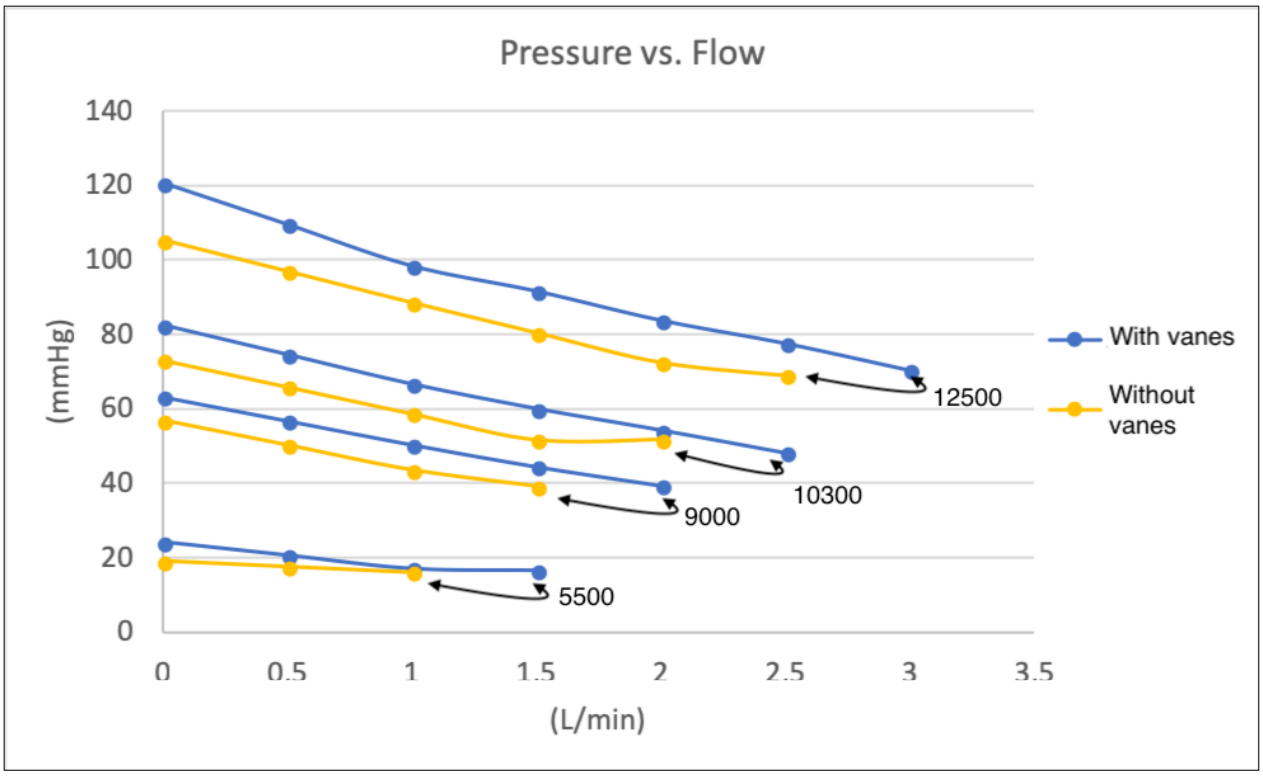

Figure 17 - Pressure - Flowrate characteristic curves for volute with and without vanes obtained by simulation.

The results confirmed that the volute without vanes presented lower pressure and flow in relation to the volute with vanes in the same rotations. The analyses showed different hydrodynamic performances. Then, it can be said that the volute with vanes is better for left ventricular assistance, providing physiological pressure and flow at lower rotations. From now on, the studies will be based on a volute with vanes. These vanes have not been optimized but it was verified that the presence of the vanes improves the performance of the pump.

4.2. Fluidodynamic Analysis

After the simulation made in ANSYS CFX software, the average pressure difference ($\Delta P = P_2 - P_1$) was obtained at the inlet and outlet, in mmHg, of all pumps. All flowrates and rotations were inserted in a table in order to generate a Pressure (mmHg) x Flow (L/min) curve, for comparison with the results of the *In Vitro* test, Table 7.

Table 7 - Simulation data.

		1Rev	2Rev	4_2	Golden	Debakey	Em2	Em3
(rpm)	(L/min)	Pressure (mmHg)						
12500	0	120.6	131.0	87.6	68.3	106.1	67.3	108.4
	0.5	109.5	116.8	80.4	60.8	97.5	60.2	104.3
	1	98.4	102.6	73.2	53.3	88.9	53.1	100.2
	1.5	91.6	90.0	65.9	45.9	85.6	46.8	98.8
	2	83.8	70.9	60.2	39.3	78.4	41.8	87.4
	2.5	77.6	67.7	56.3	40.6	74.5	37.8	83.0
	3	70.4	59.5	50.0	36.0	72.8	34.0	78.3
10300	0	82.4	89.5	60.1	46.9	79.1	46.1	80.0
	0.5	74.5	78.1	54.2	40.8	71.0	40.2	75.0
	1	66.6	66.7	48.3	34.7	62.9	34.3	70.0
	1.5	60.0	50.3	43.4	28.9	55.7	29.6	65.0
	2	54.2	48.7	39.1	28.7	52.3	26.0	59.5
	2.5	48.1	43.6	34.1	24.8	54.2	25.4	53.5
	3	42.6	36.4	30.0	22.6	52.9	22.8	48.9
9000	0	63.1	68.7	46.3	36.0	62.0	35.2	62.0
	0.5	56.7	58.9	41.7	30.8	54.6	30.2	57.3
	1	50.3	49.1	37.1	25.6	47.2	25.2	52.6
	1.5	44.4	39.7	32.5	24.4	42.4	21.4	48.2
	2	39.3	36.9	28.0	20.4	38.7	18.5	43.3
5500	0	24.1	20.9	16.6	17.2	24.3	11.0	23.8
	0.5	20.6	19.0	14.8	13.3	20.5	10.6	20.7
	1	17.1	17.1	13.0	9.4	16.7	10.2	17.6
	1.5	16.6	16.9	10.6	7.3	16.2	9.1	14.9

Subsequently, the Pressure x Flow curve was generated for each rotor, according to Figures 18 ~ 24.

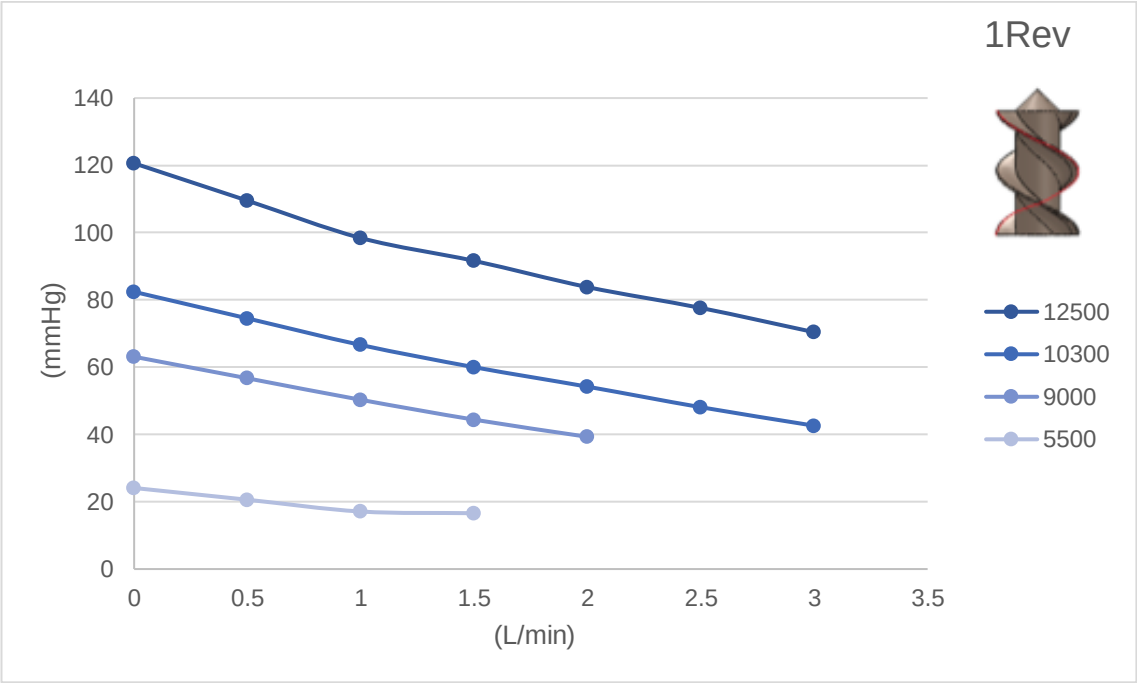

Figure 18 - Pressure Vs. Flow Curve to Rotor 1Rev.

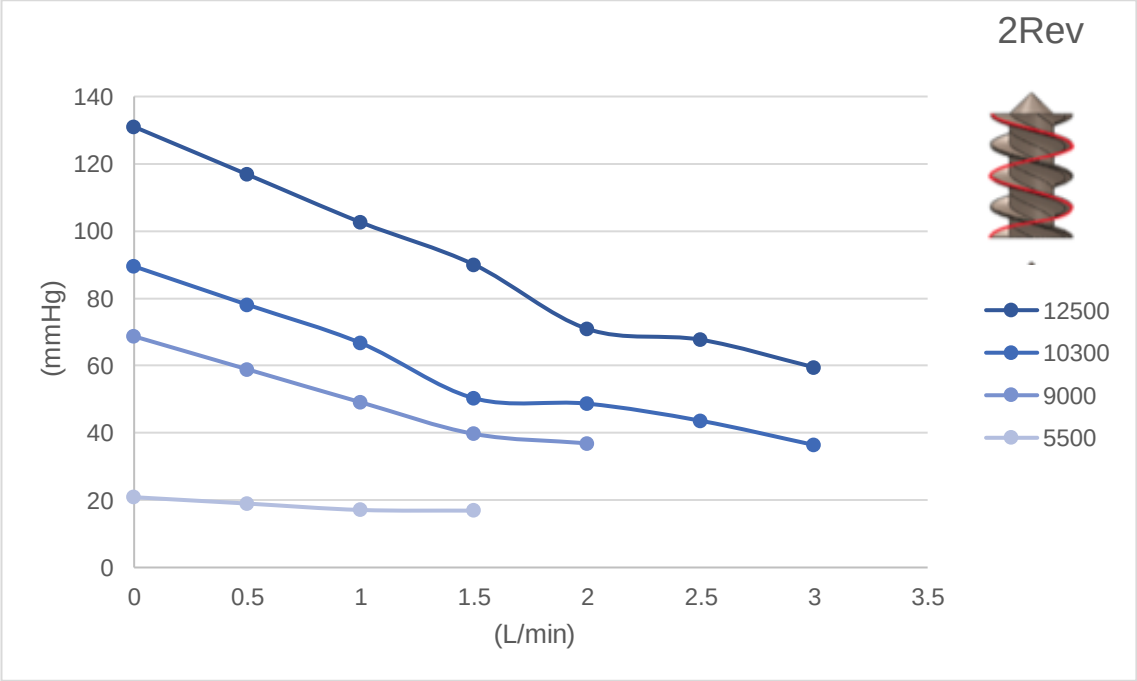

Figure 19 - Pressure Vs. Flow Curve to Rotor 2Rev.

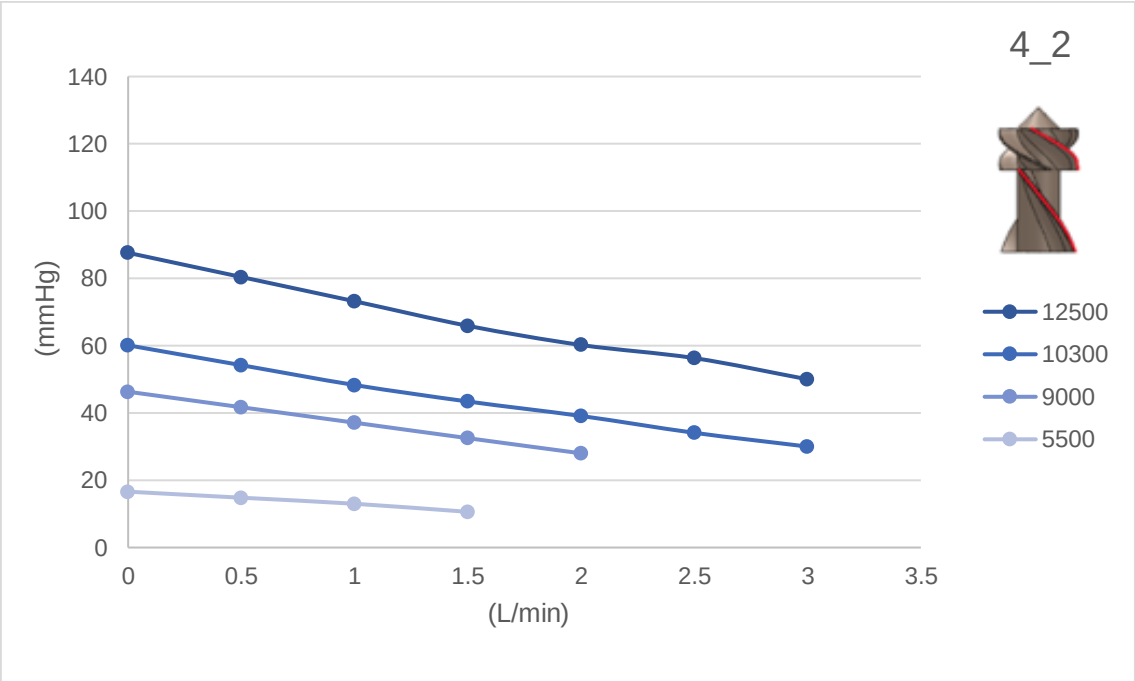

Figure 20 - Pressure Vs. Flow Curve to Rotor 4_2.

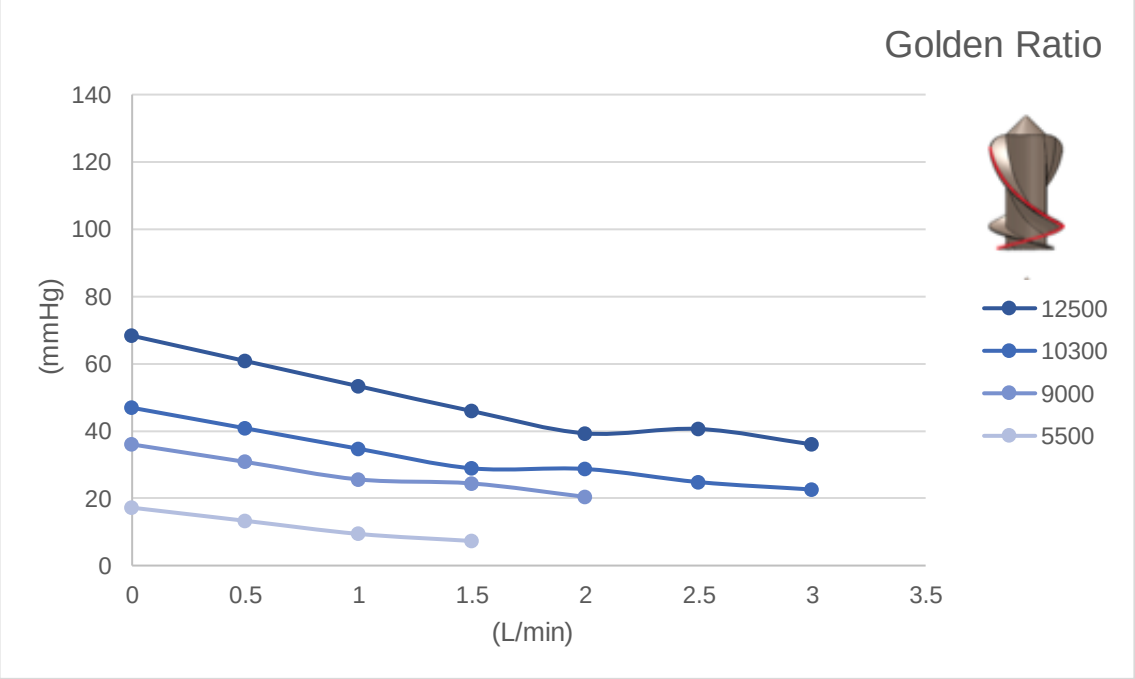

Figure 21 - Pressure Vs. Flow Curve to Rotor Golden Ratio.

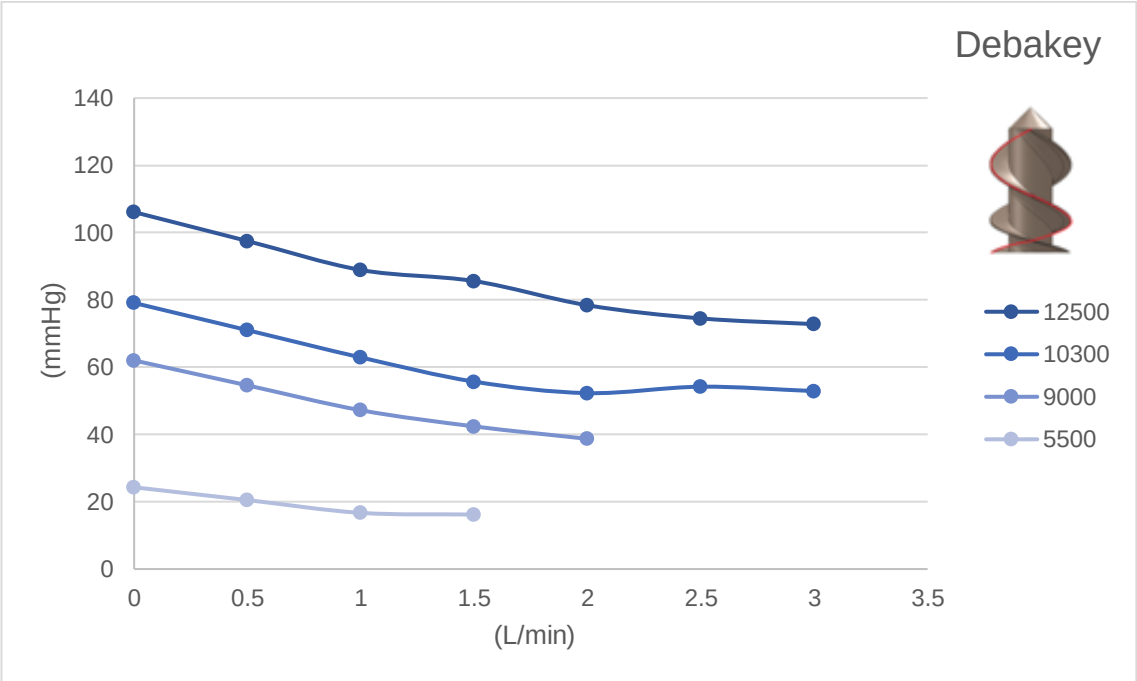

Figure 22 - Pressure Vs. Flow Curve to Rotor Debakey.

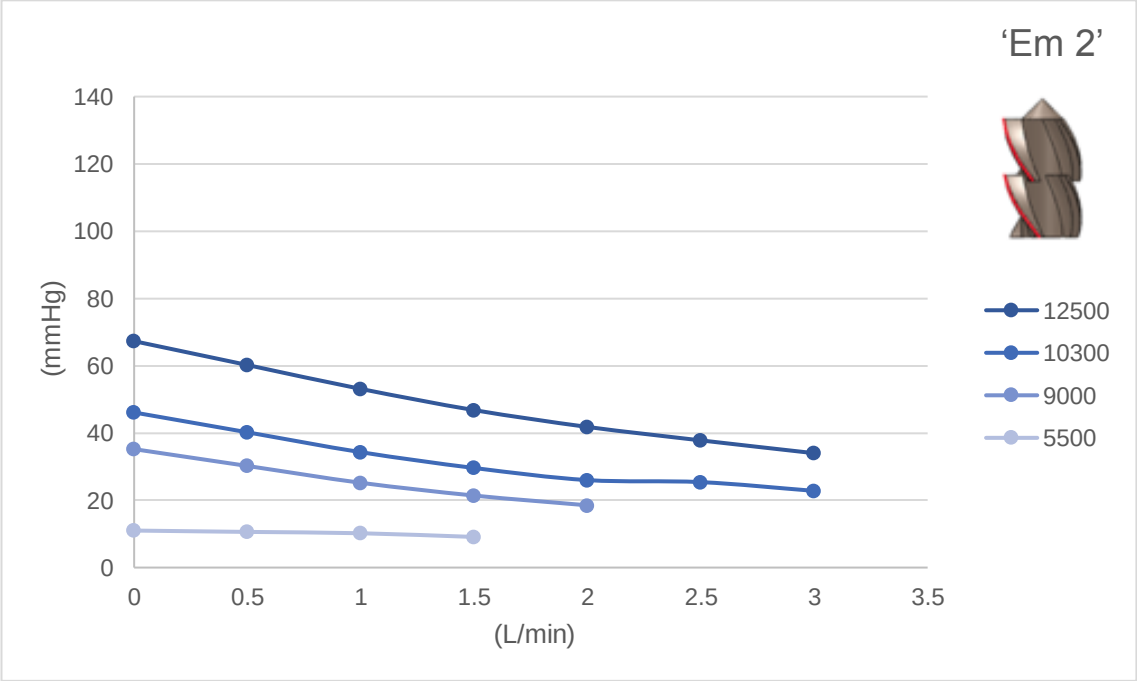

Figure 23 - Pressure Vs. Flow Curve to Rotor Em2.

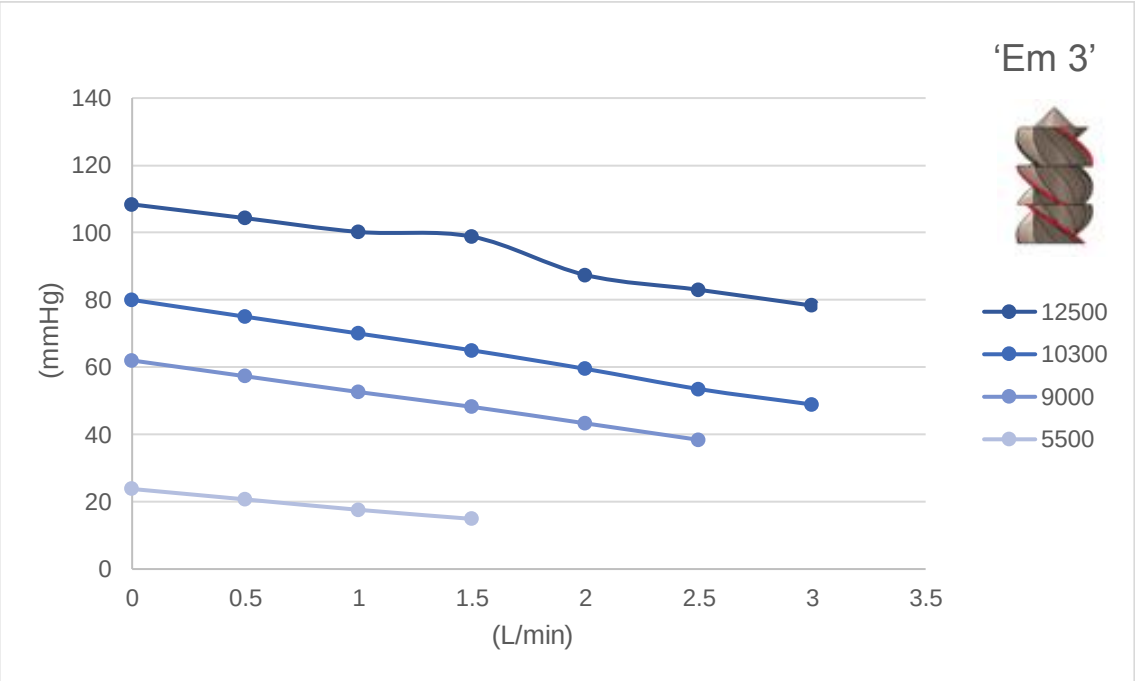

Figure 24 - Pressure Vs. Flow Curve to Rotor Em3.

Simulations showed that the rotors with better hydrodynamic performance were those named as 1Rev, 2Rev and Em3, for high rotations and low flow; 1Rev, Debakey and Em3, for high rotations and high flow as well as for low rotations and low flow and 1Rev, 2Rev and Debakey for low rotations with medium flow. Thus, the subsequent tests were performed only for the 1Rev, 2Rev, Debakey and Em3 rotors.

4.3. Shear Stress

The shear stress values were obtained for the four proposed rotor models (1Rev, 2Rev, Debakey and Em3), because they were the rotors that presented the best performance in fluid dynamics analysis by CFD. Table 8 shows the highest and the lowest shear rates found for each rotor and the average time for a particle to pass through the pump, under equal conditions.

Table 8 - Shear stress and exposure time for each rotor.

Rotor	Shear Strain Rate (s^{-1})	Effective Shear (Pa)	Time (s)
1Rev	134253	470	0.037
	42482	149	0.085
2Rev	458855	1606	0.047
	135306	474	0.108
Debakey	106591	374	0.041
	46017	161	0,091
Em 3	106568	373	0.035
	32030	112	0.071

The effective shear is calculated from equation VII (Section 2.4), inserting the data already presented and the shear strain rate that is variable. Hemolysis occurs when the product of shear stress and the exposure time exceeds a critical value. Comparing Table 8 with the reference values shown in Table 3, all four rotors presents some amount of hemolysis.

And plotting these values in the Exposure time vs Shear curve, the effective shear and the exposure time, the 2Rev rotor shows the highest shear, followed by 1Rev, and the lowest shear is found in the Debakey and Em3 rotor, Figure 25. It is expected that all four rotors present some amount of hemolysis. This is only an estimate, since the time considered is not the exposure time, but the time for the particle to arrive from the inlet to the outlet of the pump.

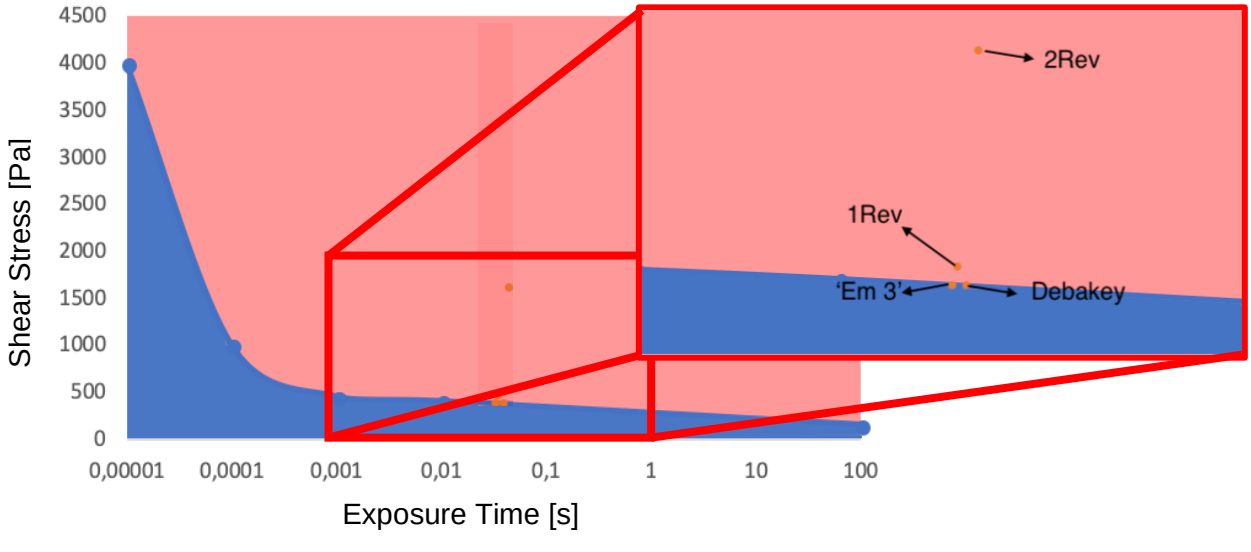

Figure 25 - Plotted values

4.4. Flow Analyses

For the flow analysis, a transverse plane was created inside the pump, passing through its center. In this plane, fluid velocities were represented using a multicolored scale, different for each rotor. One thousand velocity vectors were inserted equally spaced to analyze the direction of the flow. Each vector was projected on the surface of the plane created to observe only variations in 2 axes, facilitating the visualization.

It can be observed that there is recirculation for all the rotors and that at low rotations (5500 rpm) the profile of the recirculation is the same (Figure 26), independent of the rotor that is being analyzed. The recirculation goes from the region just above the blade until the exit of the volute. Otherwise, for high rotations (12500 rpm), the profile changes and the recirculation reduce for all analyzed rotors (Figure 27). The rotor 1Rev presents a flow circulation just above the blade and another close to the top of the rotor. The rotors 2Rev and Em3 present only one circulation just above the blade. Finally, the rotor Debakey presents a great recirculation that goes from the region, just above the blade, until the exit of the volute. Thus, in this case, the Em3 and the 2Rev presented the lowest recirculation.

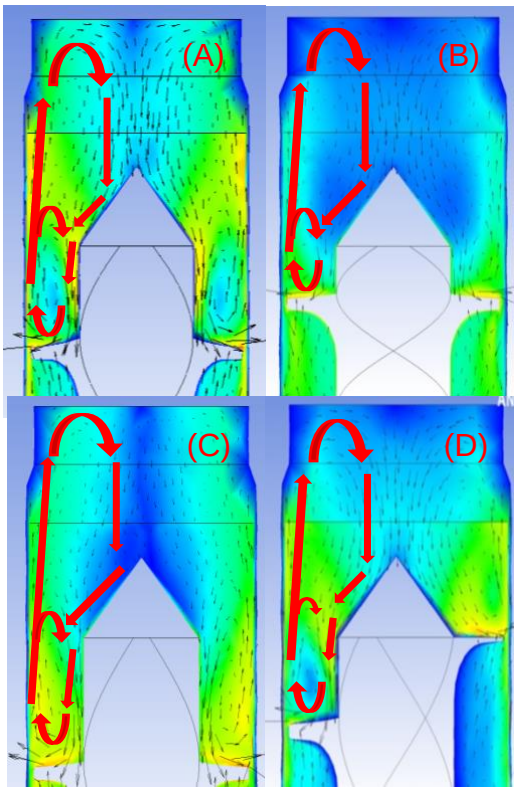

Figure 26 - Recirculation profile at 5500rpm for (A) 1Rev, (B) 2Rev, (C) Debakey, (D) Em3.

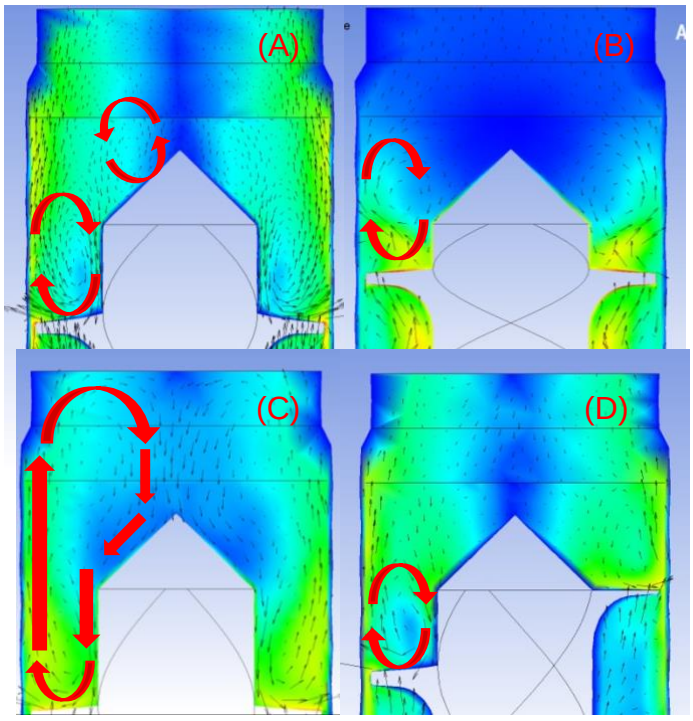

Figure 27 - Recirculation profile at 12500rpm for (A) 1Rev, (B) 2Rev, (C) Debakey, (D) Em3.

Next, the pressure distribution in the pump volute (Figure 28) was analyzed to confirm the statement made in Mizuguchi, 2018, that the continuous rotor eliminates high negative pressure zones.

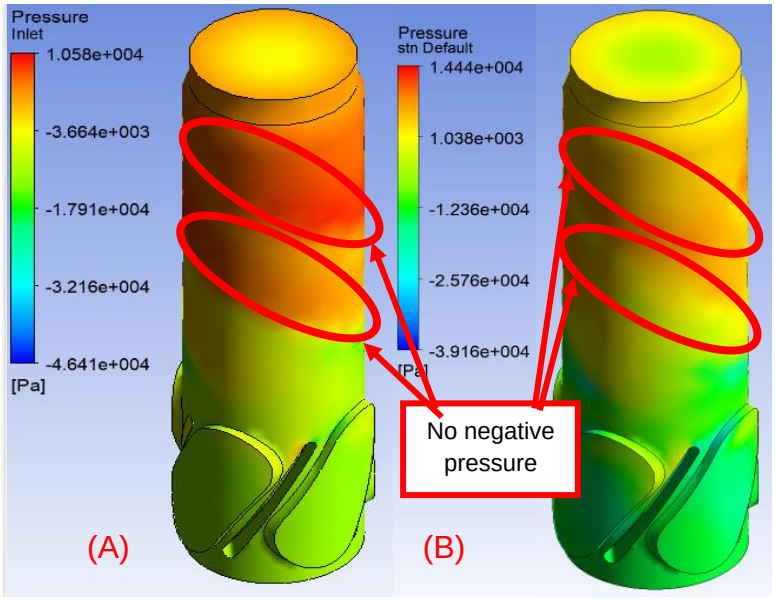

Figure 28 - Pressure Distribution on the volute (A) 1Rev, (B) Em3.

4.5. Gap Influence

Studies were also carried out on the influence of the distance or gap between the top of the blade and the volute. To this end, a rotor with a gap smaller than the one already used in this study was modeled, with the objective of reducing the pump internal leakage, as described in Schabowski *et al*, 2007. In the first rotor, the minimum distance from the blade to the volute was of 0.46 mm, while in the rotor with the reduced gap, the minimum distance was of 0.3 mm, 35% smaller.

When making the flow analysis (Figure 29), it is verified that the rotor with a larger gap presents a more accentuated internal leakage, while the rotor with smaller gap presents almost no internal leakage and the velocity vector at the top of the blade is directed upwards.

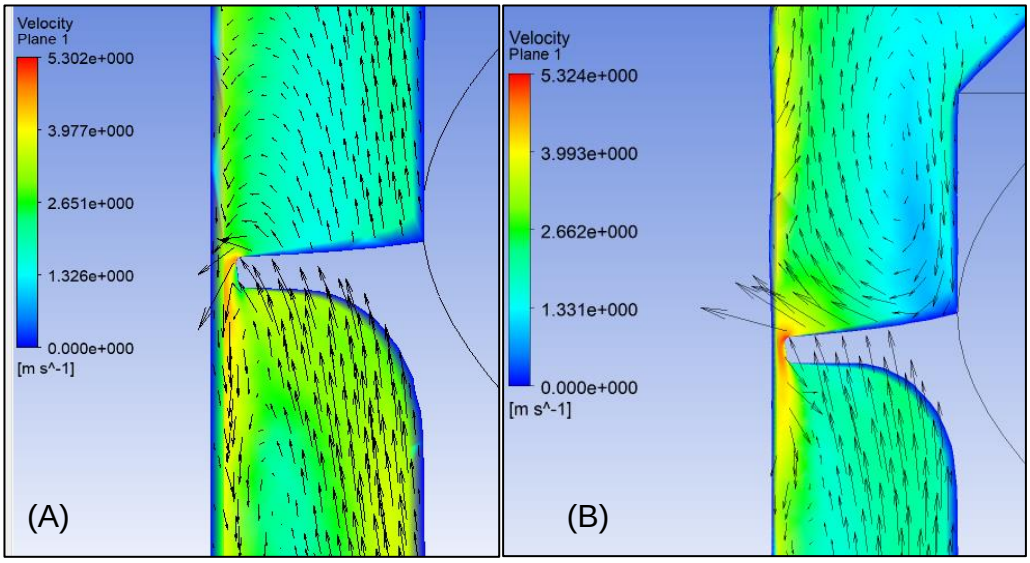

Figure 29 - Flow analysis for the rotor with gap of (A) 0.46 mm and (B) 0.30 mm.

It was generated the curve of pressure load vs. flow for both gaps and the generated curves were superimposed in Figure 30. These results showed that there is an average pressure gain of approximately 7% when the gap decreases, most of this gain is observed for larger flows and for low flows there is almost no change. However, when comparing the values of the effective maximum shear stresses, there is an increase of 45%, going from 470.31 Pa in the 0.46 mm gap, to 681.19 Pa in the 0.30 mm gap. When balancing the impact of the performance gain and shear stress, it is concluded that 0.46 mm is better in this case.

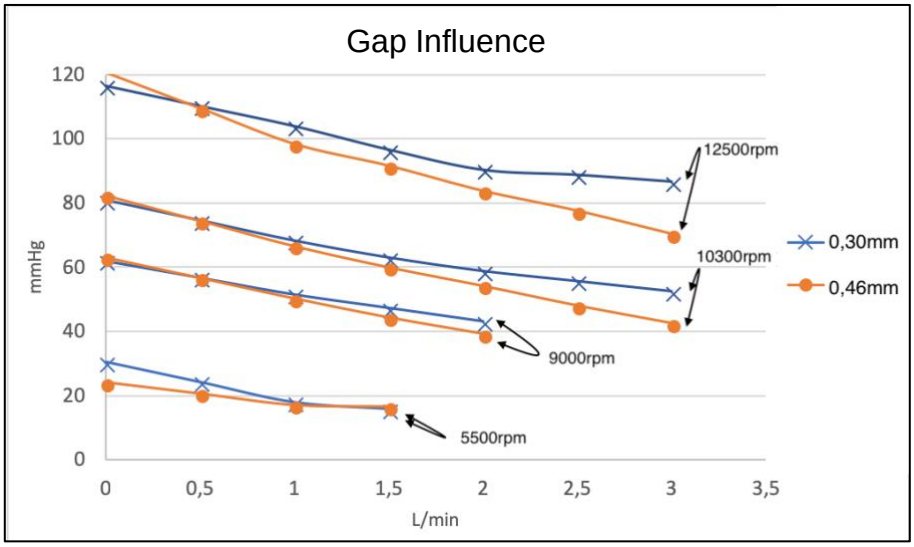

Figure 30 - Comparative gap influence curve.

5. *IN VITRO* TESTS

In this chapter, the steps to perform the *In Vitro* tests will be presented, including the construction of the prototypes to be studied, the creation of an Evaluation Unit (EU), the pressure vs. flow curves generated by the test and a comparison of the test with blood analog fluid.

5.1. Construction of Prototypes of the TVAD

These prototypes were built using fast prototyping or 3D printing technology, Polyjet (Connex® 350, Objet Geometrics, Israel) which is available at IDPC. To construct three-dimensional physical models, this equipment uses a system of heads that deposits resin droplets on a construction platform. After depositing each layer, an ultraviolet light is applied to cure the resin layer. The same procedure is done for all layers until the prototype is completed (Leme, 2015).

The process uses a resin as building material and a gel as support material. After completing the prototype, the support material is easily removed with a water jet. The prototypes built by this method have practical surface finish and mechanical strength.

The 3D printer to be used in this project is capable of building prototypes using different materials with different mechanical properties. The materials are deposited in very thin layers (16 μm) in order to build the prototype from layer to layer.

Some components of the pump were printed in order to perform the assembly of the unified prototype of the TVAD. These components include the volute with, Figure 31(a), and without vanes at the inlet, Figure 31(b), the different types of rotors to be tested, **Error! Reference source not found.**2, and the valves, **Error! Reference source not found.**3, although it will not be used. These components were printed in 3D due to the fact that their geometry is very complex for the conventional machining.

Figure 31 - (a) Volute without vanes and (b) Volute with vanes.

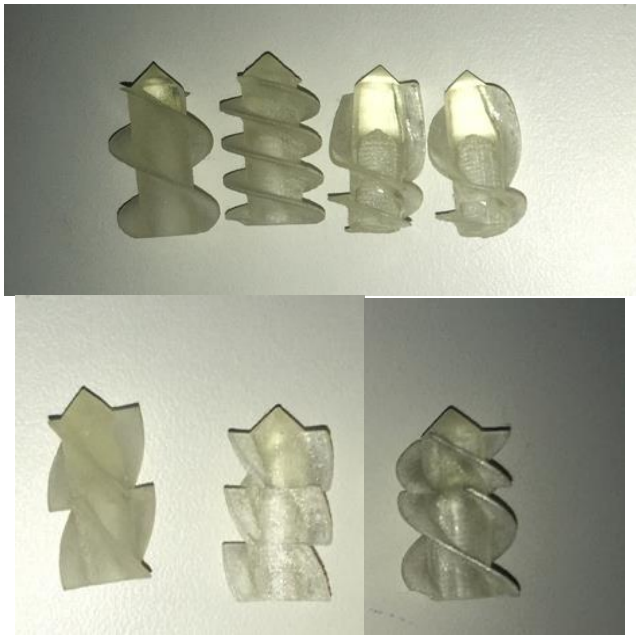

Figure 32 - Different geometries of rotors to be tested.

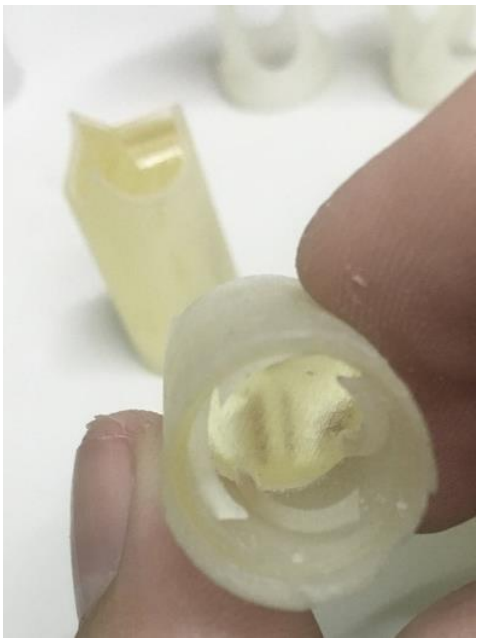

Figure 33 – Valves

Other simpler components such as the axle (in stainless steel) that connects the motor to the rotor and the motor cover (in Delrin or polyacetal) were machined on a conventional lathe at CEAC-IDPC, according to Figure 34.

Figure 34 - Motor cover, axle and rotor mounted near the motor.

After preparing all components, including the TVAD motor, the unified prototype was assembled, Figure 35.

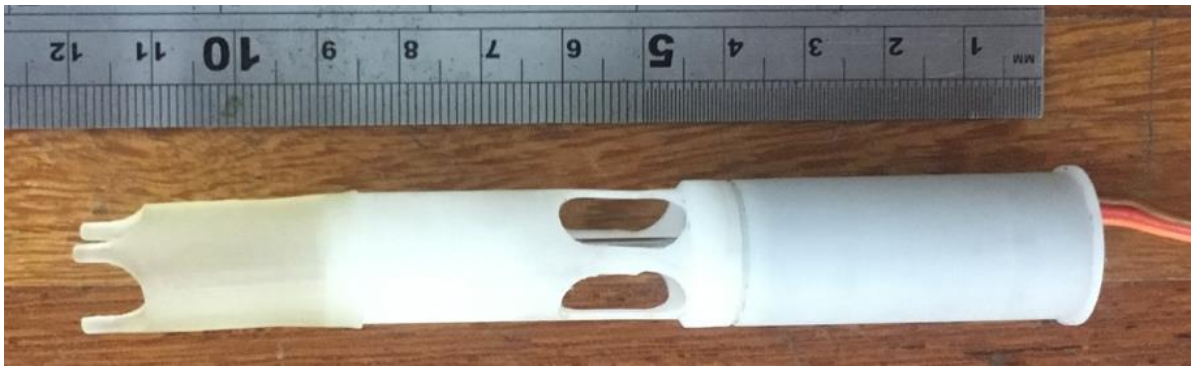

Figure 35 - Assembled Prototype.

5.2. Development of an Evaluation Unit

For In Vitro tests of the TVAD, an Evaluation Unit (EU) was developed. The EU enables a better parametrization of tests besides enabling the use of a spare motor, instead the specified one, designated to the final version of TVAD. The EU was developed to work also in combination with the Hybrid Cardiovascular System Simulator (HCSS), used at IDPC on testing devices to be applied in the cardiovascular system, Figure 36 (Fonseca, 2012).

The EU and some cannulas were machined in acrylic due to its resistance and transparency, enabling the visualization of internal components such as: the rotor in operation, the valve, the presence of bubbles and the test fluid. A stainless-steel axle is used to connect the motor to the axial rotor, being supported by two bearings for centralization. Two retainers are used to prevent air from entering or any test fluid leakage, keeping the motor isolated from this fluid.

Figure 36 - Evaluation Unit combined with the HCSS

Figure 37 shows the exploded view of the EU containing the axle, with bearings and retainers, the rotor being tested and the motor. As this is a rigid unit, it is important that the distance between the inlet and outlet of the EU is precisely respected, according to the dimensions of the HCSS.

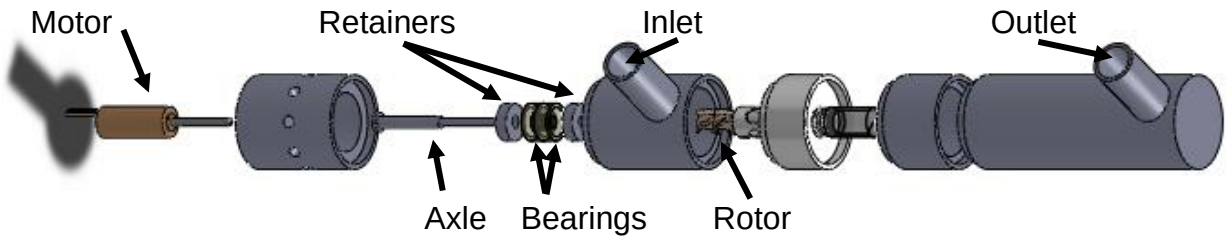

Figure 37 - Exploded view of the EU.

5.3. Conducting the Tests

Hydrodynamic performance tests were conducted at CEAC, Bioengineering Department of IDPC. The objectives of these tests were to know the hydrodynamic characteristics of each prototype, through the generation of the pressure gain vs. flow curves (ΔPxF) for different rotations.

As shown in Figure 38, the circuit used is composed of a reservoir, 3/8" PVC flexible tubes (Nipro Medical, Sorocaba, Brazil), a clamp (FAJ, São Paulo, Brazil) for flow and pressure variation, the EU and the prototype to be tested.

The flow rate was measured by an ultrasonic flowmeter for 3/8" tubes, located at the pump outlet (HT110, Transonic System, Ithaca, NI, USA), and the pressure by two invasive pressure transducers (Dome®, GabMed, São Paulo, Brazil) and one Polygraph (SP12, TEB, São Paulo, Brazil) (Figure 39), being the Inlet pressure called Pressure 1 (P1) and the Outlet pressure called Pressure 2 (P_2).

With pressure transducers, it was possible to measure the difference between inlet and outlet pressure loads (ΔP), where: $\Delta P = P_2 - P_1$. The pump rotation is set to an initial value of 5500 rpm (equivalent to 33V) and increased in intervals of approximately 2500 rpm (or 15V). At each rotation, the flow rate and the pressure load were adjusted using the clamp. Tests were conducted at room temperature (~23ºC). A digital tachometer (Figure 40 and Figure 41) was used to measure the rotation of the pump rotor. In this test, the clamp was adjusted until the tube was completely occluded, without flow, and the maximum pressure load was determined for each rotation. As the clamp decreases the resistance in the pipe, the flow increases, decreasing the ΔP, for a certain rotation (Andrade, 1998).

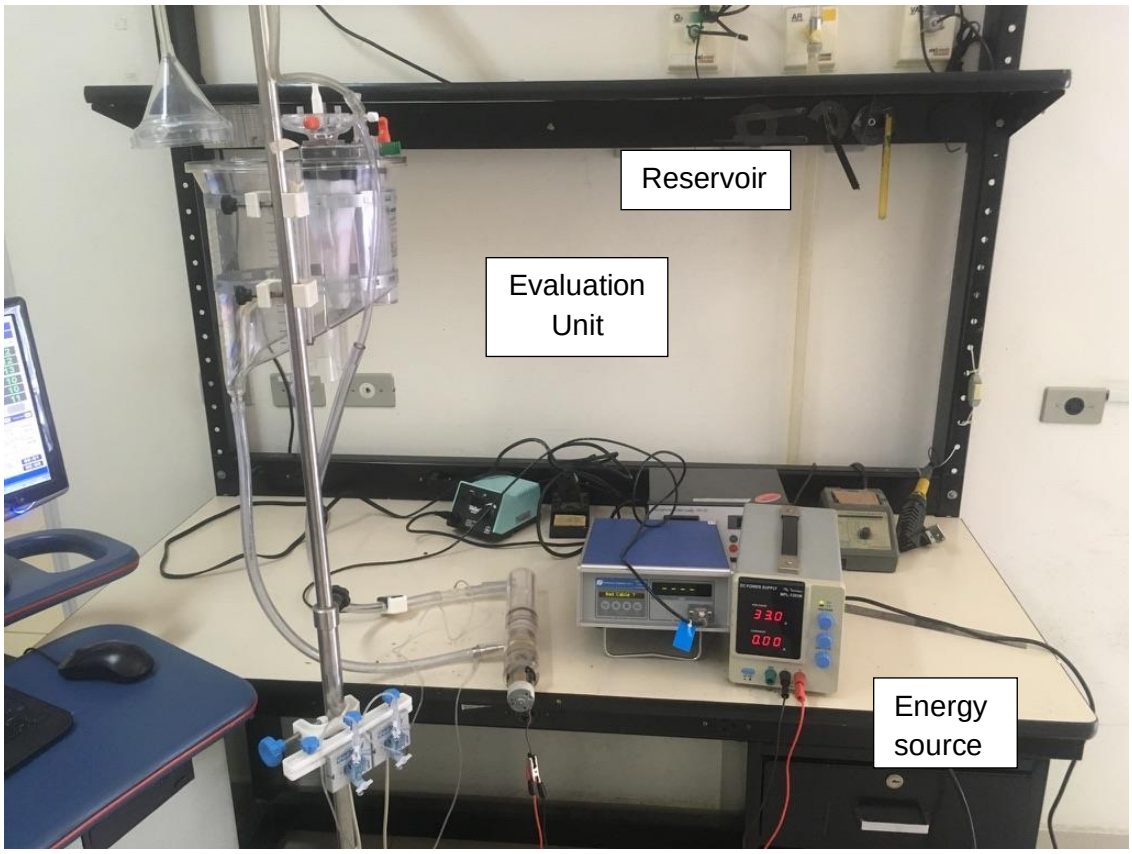

Figure 38 - Performing the test

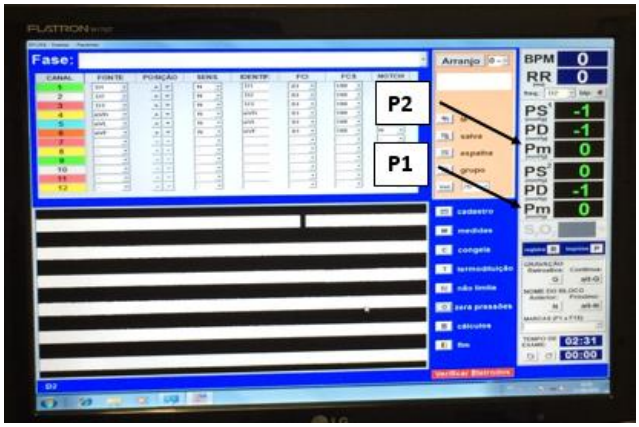

Figure 39 - Polygraph

Figure 40 - Digital tachometer

Figure 41 - Use of digital tachometer for speed measurement.

In Vitro hydrodynamic tests were performed with four proposed rotor models (1Rev, 2Rev, Debakey and Em3). These rotors presented the best performance in the simulations. During the *In Vitro* tests, the difference of the average pressure load ($\Delta P = P_2 - P_1$) was measured at the inlet and outlet, in mmHg, of all 4 pumps. All flows and rotations were inserted in a table in order to generate a curve of Pressure (mmHg) vs. Flow (L/min), for comparison with the results obtained in the simulation.

Using the test circuit, measurements of the pressure load difference (*ΔP*) and the flow, adjusted by a clamp at intervals of 0.5 L/min, were performed. With the data obtained, according to Table 9, hydrodynamic performance curves were generated for the predetermined rotations for each of the rotors, superimposed on the curves generated by the simulation, according to Figure 42 to Figure 45.

Table 9 - In Vitro tests data.

		1Rev	2Rev	Debakey	Em3
(rpm)	(L/min)	Pressure (mmHg)			
12500	0.0	126	161	124	116
	0.5	116	143	116	107
	1.0	109	132	104	96
	1.5	100	115	95	86
	2.0	90	100	83	77
	2.5	82	84	72	68
	3.0	73	71	62	57
10300	0.0	78	98	79	73
	0.5	70	84	70	64
	1.0	64	71	62	57
	1.5	57	58	53	48
	2.0	48	44	44	42
	2.5	40	33	35	31
	3.0	34	25	25	25
9000	0.0	66	76	61	59
	0.5	60	64	54	51
	1.0	53	54	48	44
	1.5	45	42	39	37
	2.0	38	32	30	29
5500	0.0	34	40	32	30
	0.5	29	31	27	26
	1.0	24	23	22	21
	1.5	20	15	15	15

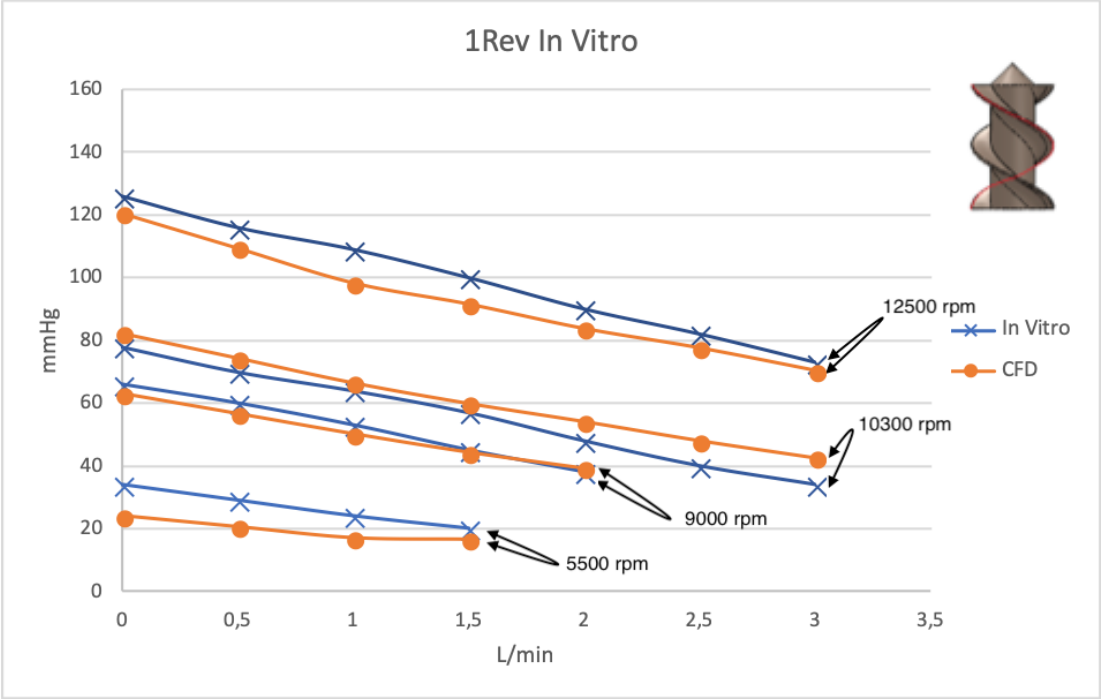

Figure 42 - Pressure Vs. Flow Curve to Rotor 1Rev - In Vitro

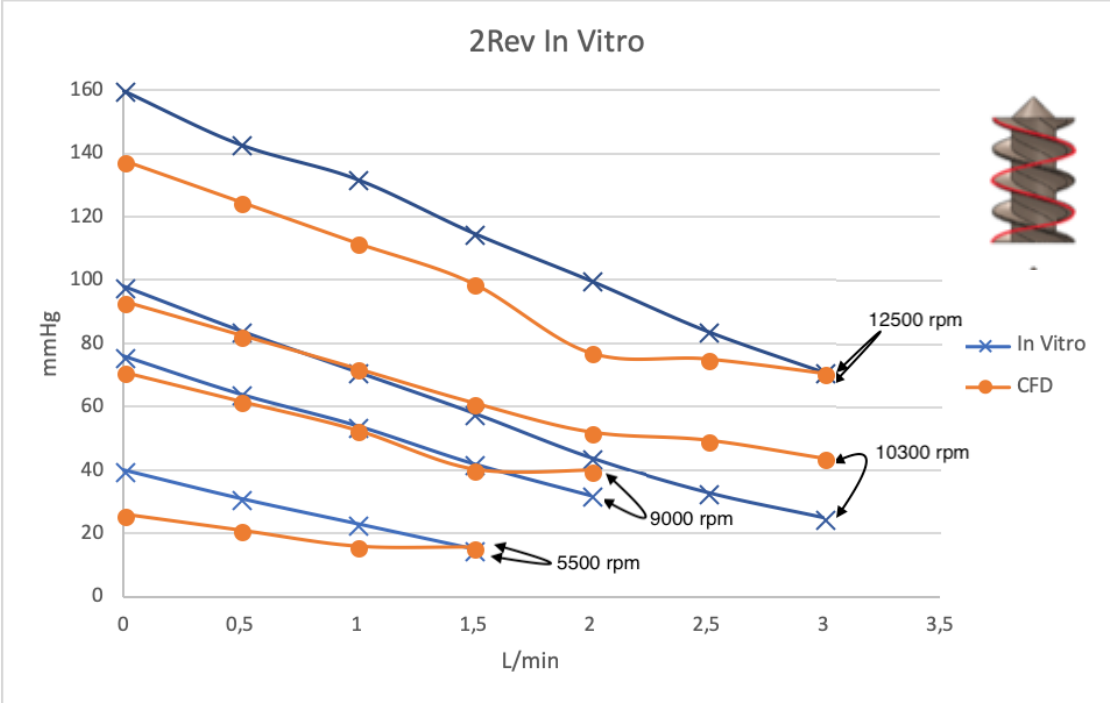

Figure 43 - Pressure Vs. Flow Curve to Rotor 2rev - In Vitro

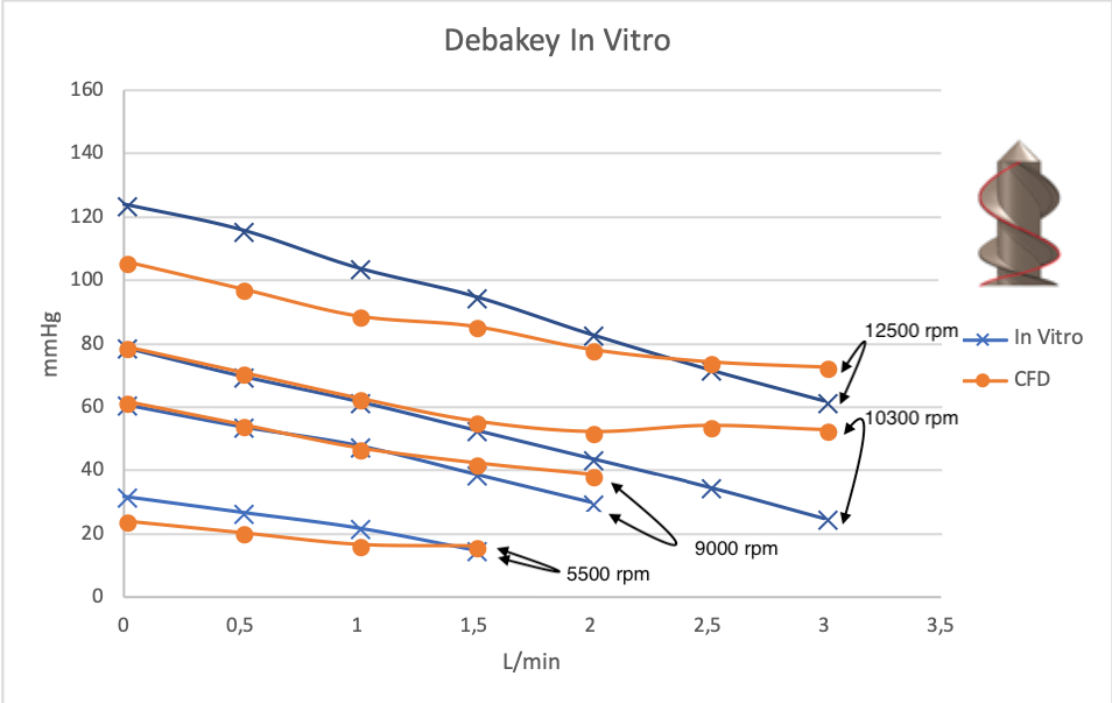

Figure 44 - Pressure Vs. Flow Curve to Rotor Debakey- In Vitro

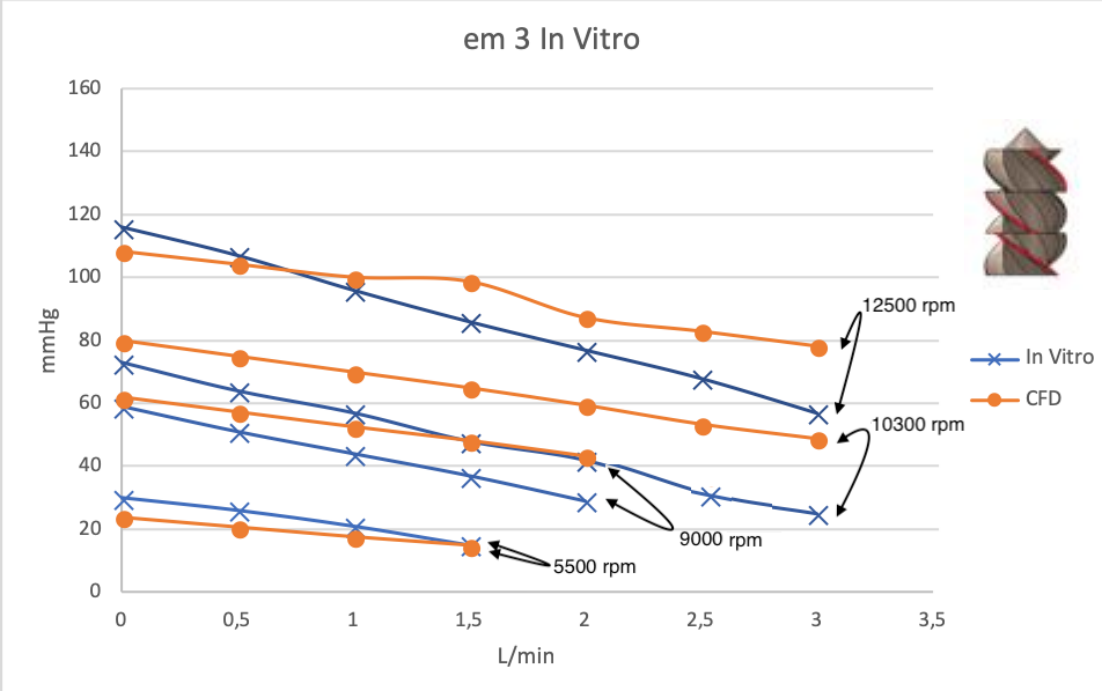

Figure 45 - Pressure Vs. Flow Curve to Rotor Em3 - In Vitro

With the hydrodynamic performance tests of the prototypes, it was possible to obtain the pressure vs. flow curves for the different rotors. These curves show that there were small pressure load differences for equal flow values between the curve generated through the simulation and the *In Vitro* test. Resulting in an average percentage error of 4% for the 1Rev rotor, 7% for the 2Rev rotor, 3% for the Debakey rotor and the most significant of 15% for the Em3 rotor. The rotors with the best hydrodynamic performance were 1Rev and 2Rev for almost all tested flows and rotations.

5.4. Blood Analogous Fluid Testing

In Vitro tests were performed also using blood analogous fluid, i.e., a mixture composed of 1/3 glycerin, 1/3 of 95% ethyl alcohol and 1/3 of distilled water (Legendre, 2008). The test was performed with the 1Rev rotor and the data obtained were compared in a pressure-flow graph, Figure 46, with the fluid being only water, for the same rotor and test circuit. From these data, it can be said that there is a pressure gain for lower flows and, for higher flows, there is no significant variation, resulting in an average difference of approximately 4% for the blood analogous fluid.

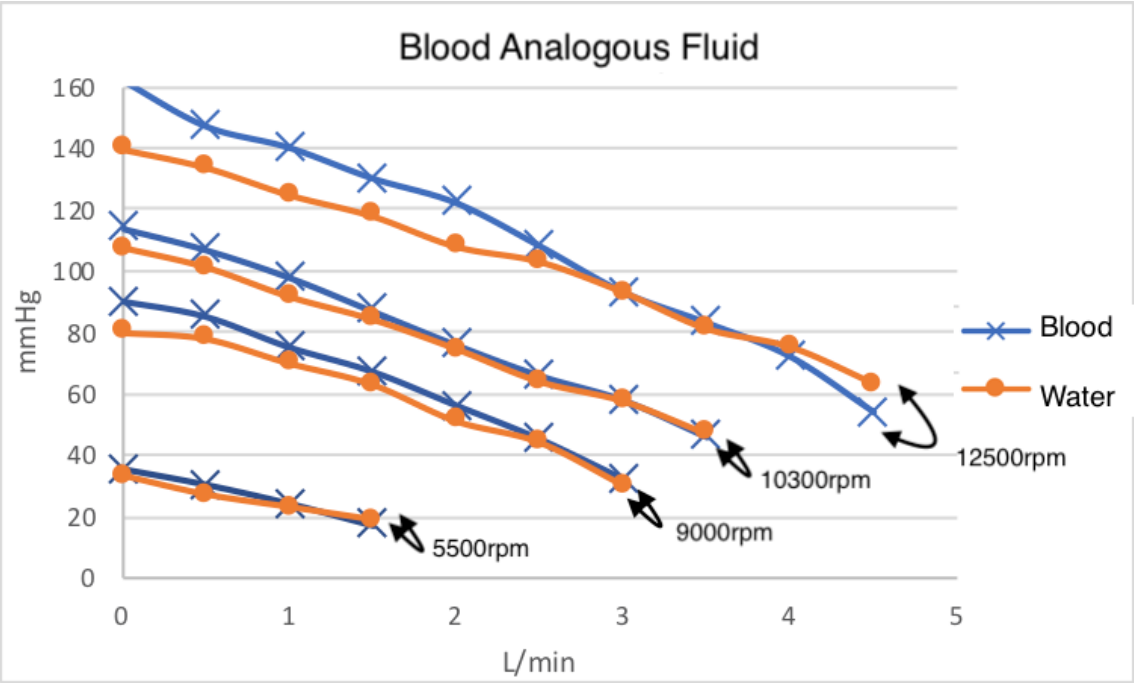

Figure 46 - Comparative chart of the blood analogous fluid.

No *In Vitro* test of the shear stress was performed. This was done only by simulation. Therefore, it is not possible to estimate the increase of the shear stress in the blood analogous fluid. The data show that the behavior of the fluids was similar to each other. With these data it can be assumed that there will be no significant change in the performance of TVAD when using blood as a fluid.

6. CONCLUSION

In this study, the analysis of the rotor geometry of an implantable axial blood pump using seven rotor of different geometries models was presented. Subsequently, comparative fluidodynamic analyses of the rotor geometries of an implantable axial blood pump were performed using the finite element method and *In Vitro* hydrodynamic performance tests. Three-dimensional models of the implantable axial blood pump with different geometries were developed using a 3D modeling software. Different rotors were tested to study the influence of the pitch of the rotor, continuous or variable pitch, the influence of the existence of two or three rows of blades with different pitch and the influence of the number of blades.

Joining all the data obtained it is assumed that the best rotor, among the rotors tested and studied, was the rotor with 2 blades arranged at 180º, continuous (only one column of blades) and with the blade pitch being constant, the 1Rev rotor. This one presented, at 12500 rpm, a maximum head of 126 mmHg, a maximum flow of 4.5 L/min. This suggest that: (I) the higher the blade pitch, the higher the pressure load, the lower flow rate, and increases shear stress; (II) a variable pitch decrease the pump efficiency and (III) a non-continuous blade decreases significantly the pump's hydrodynamic performance and decreases the shear stress.

Also, according to CFD analysis, it is expected that this rotor presents an acceptable index of hemolysis (NIH). In a nutshell, it is expected that better conditions to pump blood is achieved using rotors with: constant pitch, high pitch value and low number of blades.

For future work it is expected to analyze TVAD anatomical placement, optimize the volute vanes, to possibly add a diffuser at the outlet improving efficiency and to build titanium prototypes to be able carry out In Vitro Hemolysis tests and acute In Vivo tests.

7. REFERENCES

Andrade, A.: "***In vitro* and *in vivo* design, prototype and testing of a new total artificial heart model by electromechanical principle of operation**". PhD diss., Unicamp, 1998.

Andrade, A. and Andrade, G.: "**Transventricular Assist Device (TVAD) - *In vitro* evaluation of a new axial blood pump using polymeric valve for rotational speed reduction**". In: 44th ESAO and 7th IFAO Congress, 2017, Viena. *Int J Artif Organs*: 40(8):430-469, 2017.

ANSYS , INC. Release 11.0 *Documentation for ANSYS*, 2007.

Autodesk, extracted from https://knowledge.autodesk.com/support/cfd/learn-explore/caas/CloudHelp/cloudhelp/2014/ENU/SimCFD/files/GUID-81E86432-7979-41AF-A7C2-9123144FC6F9-htm.html in 07th may of 2018.

Avezum, A., Maia, L.N. and Nakazone, M.: "**Cenário das Doenças Cardiovasculares no Mundo Moderno**". In: Timerman, A.; Bertolami, M. and Ferreira, J.F.M. *Manual de Cardiologia*. São Paulo: Editora Atheneu, pag. 1-5, 2012.

Baliga, B.R. and Patankar, S.V.: "**A control-volume finite-element method for two-dimensional fluid flux and heat transfer**". *Numerical Heat Transfer*, 6(1):245- 261, 1983.

Baliga, B.R. and Patankar, S.V.: "**A new finite-element formulation for convection-diffusion problems**". *Numerical Heat Transfer*, 3(1):393-409, 1980.

Bock, E.; Ribeiro, A.; Silva, M.; Antunes, P.; Fonseca, J.; Legendre, D.; Leme, J.; Arruda, C.; Biscegli, J.; Nicolosi, D. and Andrade, A.: "**New centrifugal blood pump with dual impeller and double pivot bearing system: wear evaluation in bearing system, performance tests and preliminary hemolysis tests**. *Artificial Organs*, 32(4):329-333, 2008.

Burgreen, G.W.; Antaki, J.F.; Wu, Z.J. and Holmes, A.J.: "**Computational fluid dynamics as a development tool for rotary blood pumps**. *Artificial Organs*, 25(1):336-340, 2001.

Chan, C.H.; Pieper, I.L.; Hambly, R.; Radley, G.; Jones, A.; Friedmann, Y.; Hawkins, K. M.; Westaby, S.; Foster, G. and Thornton, C.A.: "T**he centrimag centrifugal blood pump as a benchmark for *in vitro* testing of hemocompatibility in implantable ventricular assist devices**. *Artificial Organs, online version* published jul, 2014. Disponible at: onlinelibrary.wiley.com/doi/10.1111/aor.12351 Acess in: August 2014.

Connellan, M.; Iyer, A.; Robson, D.; Granger, E.; Dhital, K.; Spratt, P. and Jansz, P.: "**The heartware transvalvular miniature ventricular assist device used for right**

ventricular support. In: *ISHLT 33rd Annual Meeting & Scientific Sessions*, 24 to 27 April, Montreal, 2013.

Dinkhuysen, J.J.; Cipullo, R. and Rossi, Neto: "**Tratamento cirúrgico da Insuficiência Cardíaca – Ventriculectomia**, Aneurismectomia. In: Timerman A, Bertolami M, Ferreira JFM. *Manual de Cardiologia*. São Paulo: Editora Atheneu, 1(1):83-88, 2012.

Fonseca, J.; Andrade, A.; Utiyama, B.; Uebelhart, B.; Leme, J.; Silva, C.; Biscegli, J.; Lucchi, J.: "**Hybrid Cardiovascular Simulator Performance Evaluation**". In: 7º COLAOB, 2012, Natal. 2012.

Gölcü, M. and Pancar, Y.: "**Investigation of performance characteristics in a pump impeller with low blade discharge angle"**. *World Pumps*. 2005; 2005(468):32-40, 2005.

Gulich, J.F.: "**Impact of three-dimensional phenomena on the design of rotodynamic pumps"**. In: *Proceedings of The Institution of Mechanical Engineers Part-C Journal of Mechanical Engineering Science*, 213(1):59-70, 1999.

Hernandes, M.; Lopes, G.; Bock, E.: "**Escoamento Sanguíneo Em Dispositivos De Assistência Ventricular: Simulação Computacional E Validação**". In: 5ª Edição Do Workshop De Biomateriais, Engenharia De Tecidos E Orgãos Artificiais - Obi, 2017, Maresias. 2017.

Hochareon, P.; Manning, K.B.; Fontaine, A. A.; Tarbell, J.M. and Deutsch, S.: "**Correlation of *In Vivo* Clot Deposition With the Flux Characteristics in the 50 cc Penn State Artificial Heart: A Preliminary Study"**. In: *ASAIO Journal*. 50(3):537–542, 2004.

ISO 14708-5: *International Standard. Implants for Surgery – Active implantable medical devices – Part 5: Circulatory support devices*. 2010.

Kanpur, I.: extracted from http://nptel.ac.in/courses/112104117/37 in 03rdjuly 2018.

Legendre, D.; da Silva, O.L.; Andrade, A.; Fonseca, J.; Nicolosi, D. and Biscegli, J.: "**Endurance Tets on a Textured Diaphragm for the Auxiliary Total Artificial Heart (ATAH)"**. *Artificial Organs*, 27(5): 457-460, 2003.

Legendre, D.; Fonseca, J.; Andrade, A.; Biscegli, J. F.; Manrique, R.; Guerrino, D.; Prakasan, A. K.; Ortiz, J. P.; Lucchi, J. C.: **"Mock circulatory system for the evaluation of left ventricular assist devices, endoluminal prostheses, and vascular diseases**". *Artificial Organs*, 32(6):461–467, 2008.

Leverett, L.B.; Hellums J.D.; Alfrey C.P. and Lynch E.C.: "**Red Blood Cell Damage by Shear Stress"**. *Biophysical Journal*. 12(3):257–272, 1972.

Leme, J.: “**Desenvolvimento e estudo *In Vitro* de um dispositivo de suporte circulatório temporário**”. Doctoral thesis, *University of São Paulo*. 2015.

Maliska, C.: “**Transferência de calor e mecânica dos fluidos computacional”**. Segunda Edição. *Livros Técnicos e Científicos Editora S. A.*, Rio de Janeiro, 2004.

Mizuguchi K.; Damm G.; Benkowsky R.; Aber G.; Bacak J.; Svjkovsky P.; Glueck J.; Takatani S.; Nosé Y. and Noon G.P.: “**Development of an Axial Fluxo Ventricular Assist Device: *In Vitro* and *In Vivo* Evaluation”**. *Artificial Organs*. 19(7):653-659, 2008.

Morales, M.M.: “**Modelagem Matemática da Fluidodinâmica Não-Newtoniana e Bifásica Simplificada da Hemólise Induzida Mecanicamente em Sistemas de Bombeamento Centrífugo de Sangue”**. *Doctoral thesis*. USP - Instituto Dante Pazzanese de Cardiologia. São Paulo. 2017.

Nosé, Y.: “**Cardiac Prosthesis Utilizing Biological Material”**. *The Journal of Thoracic and Cardiovascular Surgery*, 62(1):714-724, 1971.

Nosé, Y.: “**Design and development strategy for the rotary blood pump”**. *Artificial Organs*. 22(6):438-446, 1998.

Nosé, Y. and Motomura, T.: “**Cardiac Prosthesis – Artificial Heart and Assist Circulation”**. *Houston: ICMT Press*, ed.4, 238p., 2003.

Oliveira, A.C.A.: “**Metodologia de Projeto Aerodinâmico de Rotores Axiais e Otimização da Pá com base nos Efeitos de Sweep e Dihedra**l”. Itajubá: Universidade Federal de Itajubá Programa de Pós-Graduação em Engenharia Mecânica. *Master dissertation*: 2014.

Olsen, D.B.: “**The history of continuos-flow blood pumps”**. *Artificial Organs*, 24(6):401-404, 2000.

Schabowski, Z. and Hodson, H.: “**The reduction of over tip leakage loss in un-shrouded axial turbines using winglets and squealer**”, *ASME Turbo Expo 2007,* Paper No. GT2007-27623, pp. 663-675, Montreal, Canada..

Shankarraman V.; Kocyildirim E.; Olia S. E.; Kameneva M. V.; Dzadony R. J.; Maul T. M.; Simon M. A.; Champion H. C.; Wagner W. R. and Bermudez C. A.: “**Biocompatibility Assessment of the CentriMag-Novalung Adult ECMO Circuit in a Model of Acute Pulmonary Hypertension”**. *ASAIO Journal*, 60(4):429-435, 2014.

Sharif R.A.L.: “**Golden Ratio in Architecture and the Human Heart”**. *International Journal of Scientific & Engineering Research*; 5(10):1529-1541, 2014.

Silva, B.U.: "**Projeto, Avaliação e Aperfeiçoamento de uma Bomba de Sangue Centrífuga Implantável Ápice Ventricular para Assistência Cardíaca**". Campinas: Faculdade de Engenharia Mecânica, *Universidade Estadual de Campinas*. Master Dissertation, 2012.

Silva, C., Silva, B.U.; Leme, J.; Uebelhart, B.; Dinkhuysen, J.; Biscegli, J. F.; Andrade, A. and Zavaglia, C.: "***In Vivo* evaluation of centrifugal blood pump for cardiopulmonary bypass – Spiral Pump**". *Artificial Organs*, 37(11):954-957, 2013

Song, X.; Throckmorton, A. L.; Untaroiu, A; Patel, S; Allaire, P.E.; Wood, H.G. and Olsen, D.B.: "**Axial Fluxo Blood Pumps**". *ASAIO Journal*, 49(1):355–364, 2003.

Souza, G.E.C.: "**Insuficiencia Cardíaca: Conceito, Diagnóstico e Classificação. In: Timerman A, Bertolami M, Ferreira JFM**". *Manual de Cardiologia*. São Paulo: Editora Atheneu, pag. 49-53, 2012.

Sudhamshu, A.R.; Pandey, M.C.; Sunil, N.; Satish, N.S.; Mugundhan, V. and Velamati, R. K.: "**Numerical study of effect of pitch angle on performance characteristics of a HAWT**". *Engineering Science and Technology, an International Journal.* 19(1):632-641, 2016.

Voorde, J.V.; Vierendeels, J. and Dick, E.: "**Fluxo simulations in rotary volumetric pumps and compressors with the fictitious domain method**". *Journal of Computational and Applied Mathematics*, 168(1):491–499, 2004.

Vosse, V.D.F.N.: "**Numerical analysis of carotid artery flow"**. Doctoral Thesis. *Technische Universiteit Eindhoven*. Eindhoven. 1987.

Wampler, R.K.: inventor, Medtronic Inc., cessionário. "**Single-stage axial flow blood pump"**, *United States patent* US4846152A. 24 Nov. 1987

Wen-Guang, L.: "**Inverse design of impeller blade of centrifugal pump with a singularity method**". *Jordan Journal of Mechanical and Industrial Engineering*; 5, p119-128, 2011.

WHO, extracted from http://www.who.int/mediacentre/factsheets/fs317/en/ in 05th January 2017.

Wilcox, David C. **Turbulence Modeling for CFD**. 2. ed. Anaheim: DCW Industries, 1998.